ER Stress-Induced Sphingosine-1-Phosphate Lyase Phosphorylation Potentiates the Mitochondrial Unfolded Protein Response

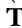Asli D. Yildirim[1,2,3] , Mevlut Citir[4] , Asli E. Dogan[1,2,3] , Zehra Veli[3], Zehra Yildirim[1,2,3] , Ozlem Tufanli[5] , Alexis Traynor-Kaplan[6,7], Carsten Schultz[8], and Ebru Erbay[1,9,10]*

[1]Smidt Heart Institute, Cedars-Sinai Medical Center, Los Angeles, CA, USA; [2]Department of Molecular Biology and Genetics, and [3]National Nanotechnology Center, Bilkent University, Ankara, Turkey; [4]Cell Biology and Biophysics Unit, European Molecular Biology Laboratory, Heidelberg, Germany; [5]New York University, Langone Medical Center, New York, NY, USA; [6]Department of Medicine, Washington University School of Medicine, Seattle, USA; [7]ATK Innovation, Analytics and Discovery, North Bend, WA, USA; [8]Department of Chemical Physiology and Biochemistry, Oregon Health & Science University, Portland, OR, USA; [9]Department of Biomedical Sciences, Cedars-Sinai Medical Center, Los Angeles, CA, USA; [10]David Geffen School of Medicine, University of California, Los Angeles, CA, USA

Abstract The unfolded protein response (UPR) is an elaborate signaling network that evolved to maintain proteostasis in the endoplasmic reticulum (ER) and mitochondria (mt). These organelles are functionally and physically associated, and consequently, their stress responses are often intertwined. It is unclear how these two adaptive stress responses are coordinated during ER stress. The inositol-requiring enzyme-1 (IRE1), a central ER stress sensor and proximal regulator of the UPR^{ER}, harbors dual kinase and endoribonuclease (RNase) activities. IRE1 RNase activity initiates the transcriptional layer of the UPR^{ER}, but IRE1's kinase substrate(s) and their functions are largely unknown. Here, we discovered that sphingosine 1-phosphate (S1P) lyase (SPL), the enzyme that degrades S1P, is a substrate for the mammalian IRE1 kinase. Our data show that IRE1-dependent SPL phosphorylation inhibits SPL's enzymatic activity, resulting in increased intracellular S1P levels. S1P has previously been shown to induce the activation of mitochondrial UPR (UPR^{mt}) in nematodes. We determined that IRE1 kinase-dependent S1P induction during ER stress potentiates UPR^{mt} signaling in mammalian cells. Phosphorylation of eukaryotic translation initiation factor 2α (eif2α) is recognized as a critical molecular event for UPR^{mt} activation in mammalian cells. Our data further demonstrate that inhibition of the IRE1-SPL axis abrogates the activation of two eif2α kinases, namely double-stranded RNA-activated protein kinase (PKR) and PKR–like ER kinase upon ER stress. ⬛ These findings show that the IRE1-SPL axis plays a central role in coordinating the adaptive responses of ER and mitochondria to ER stress in mammalian cells.

Supplementary key words adaptive stress response • endoplasmic reticulum • mitochondria • inositol-requiring enzyme-1 • endoribonuclease • kinase • eukaryotic translation initiation factor 2α • proteostasis • ire1-spl axis • signaling networks

Proteostasis entails dynamic balancing of a functional proteome through translation, protein folding, and protein degradation as cells undergo adaptation to intracellular and extracellular demands. An adaptive stress response, known as the unfolded protein response (UPR), is induced in response to the accumulation of misfolded proteins in the endoplasmic reticulum (ER) and mitochondria. UPR signaling provides a mechanism that cells can reinstate homeostasis in these organelles (1, 2). Failure or perturbation of UPR-related proteostatic mechanisms can impair cellular function and if prolonged, reduce cell viability.

The ER is the major intracellular compartment for the synthesis and folding of secreted and transmembrane proteins, calcium storage, lipid metabolism, and membrane biogenesis. Disruption of any of these functions can activate UPR^{ER} (3). Activation of UPR^{ER} initiates both transcriptional and translational layers of control that are regulated by the ER membrane-anchored stress sensors, namely inositol-requiring enzyme-1 (IRE1), double-stranded RNA-activated protein kinase (PKR)–like ER kinase (PERK), and activating transcription factor-6 (4). IRE1 is the most conserved arm of the UPR and has dual enzymatic activities, namely endoribonuclease (RNase) and kinase (5). Upon accumulation of misfolded proteins in the ER lumen, IRE1 transautophosphorylates, leading to oligomerization and robust activation of its RNase domain (6). IRE1 RNase domain splices X box-binding transcription factor-1 (Xbp1) mRNA, which translates into an active transcription factor that translocates into the nucleus to transcriptionally activate the genes encoding ER

*For correspondence: Ebru Erbay, ebru.erbay@cshs.org.

stress–related chaperons and ER-associated degradation machinery (7, 8). While the function of the IRE1 RNase domain and its target, Xbp1, in the context of UPR^{ER} is well understood, knowledge on IRE1 kinase function and substrate(s) is limited (9). Activation of the second UPR arm that is regulated by PERK kinase leads to inhibitory phosphorylation of eukaryotic translation initiation factor 2 alpha (eif2α). Besides PERK, there are three other kinases that can phosphorylate eif2α, namely heme-regulated inhibitor (HRI), general control nonderepressible-2 (GCN2), and PKR, under different stress conditions (10). eif2α phosphorylation by these kinases initiates a shared adaptive signaling known as the integrated stress response (ISR), resulting in translational attenuation. However, translation of a select group of mRNAs such as the activating transcription factor-4 (ATF4) mRNA that have upstream open reading frames in their 5′ untranslated region is enhanced. ATF4 transcriptionally regulates metabolic and cellular changes that can promote recovery from stress and cell survival (11). Other examples of mRNAs that escape from translation arrest include the transcription factors CCAAT/enhancer-binding protein homology protein (CHOP) and ATF5 (12). ATF4, CHOP, and ATF5 are also central players in the initiation of the mitochondrial UPR (UPR^{mt}) (10, 13). Intriguingly, a study has shown that IRE1 contributes to PKR activation in response to infection by *Chlamydia trachomatis*, suggesting crosstalk exists between UPR^{ER} and ISR pathways (14). Whether IRE1 has an impact on the activation of PKR or any other eif2α kinases during ER stress conditions is unknown.

Mitochondrial stress and dysfunction can induce the UPR^{mt} signaling to reinstate homeostasis in this organelle (15, 16). Activation of the mammalian UPR^{mt} requires eif2α phosphorylation, a shared stress mediator with the UPR^{ER} and ISR. It is not clear which of the four cellular eif2α kinases responds to distinct types of mitochondrial stressors or ER stress, upstream of UPR^{mt} activation (17). Phosphorylation of eif2α has several known consequences for the stressed mitochondria: i) general translation attenuation that reduces protein import and folding load in the mitochondria, ii) robust translation of ATF4 that promotes CHOP transcription and consequently, ATF4 and CHOP can induce ATF5, a central player in UPR^{mt}, iii) in combination, ATF4, CHOP, and ATF5 orchestrate the transcriptional upregulation of mitochondrial chaperones [such as mitochondrial heat shock proteins (mtHSP) 70 and 10] that assist proper protein folding and assembly of mitochondrial matrix proteins and mitochondrial quality proteases [such as Lon protease-1 (LONP1) and caseinolytic protease-1(CLPP1)] that degrade misfolded proteins and prevent proteotoxicity (18–20). In mammalian cells, ATF5, ATF4, and CHOP are all required for UPR^{mt} induction (21–23).

ER-mitochondria membrane contacts that facilitate the exchange of critical information (in the form of calcium, metabolites, and reactive oxygen species) between these organelles are important for sustaining a healthy collaboration that underlies their shared biosynthetic capability (such as phospholipid homeostasis) and other cellular roles. The dysfunction in one organelle can negatively impact the other as seen in many metabolic and inflammatory diseases (24, 25). While UPR^{ER} and UPR^{mt} share some common features (such as eif2α phosphorylation), how these organelles' adaptive stress responses are coordinated is not well understood. Classical ER stress inducers can induce the three transcriptional regulators (ATF4, ATF5, and CHOP) required for UPR^{mt} induction. Also, the expression of the mitochondrial quality protease, LONP1, is induced by ER stress in a PERK-dependent manner, implying UPR^{ER} can directly impact mitochondrial proteostasis (26, 27). PERK-induced LONP1 during ER stress leads to degradation of phosphatase and tensin homolog-induced kinase 1, a critical mitophagy regulator, which abrogates mitophagic clearance during ER stress (28). ER stress can also be induced by mitochondrial stressors. For example, paraquat (a superoxide generator that perturbs mitochondrial respiratory chain function and induces UPR^{mt}) can activate IRE1, suggesting that the IRE1 arm of the UPR^{ER} is connected to mitochondrial dysfunction (29). Whether IRE1 contributes to mitochondrial proteostasis is not known.

Many pieces of evidence suggest that ER and mitochondrial stress pathways are intertwined, but how they are coordinated is less clear. In this study, we investigated IRE1's role in ER stress-induced UPR^{mt} signaling. We discovered that IRE1 activation is required for robust UPR^{mt} signaling induction by ER stress. A recent study has shown that sphingosine 1-phosphate (S1P) lyase (SPL, encoded by *SGPL1*), the enzyme that degrades S1P into phosphoethanolamine and hexadecanal, is found in the IRE1 interactome (30, 31). As S1P has been proposed to play an upstream role in UPR^{mt} activation in *C. elegans*, we investigated whether SPL bridges IRE1 to UPR^{mt} regulation (32). Our data show that IRE1-mediated SPL phosphorylation inhibits SPL's activity, leading to accumulation of intracellular S1P. ER stress–induced and IRE1 kinase activity-dependent induction of S1P resulted in enhanced UPR^{mt} signaling. Furthermore, we demonstrate that the inhibition of IRE1-SPL axis profoundly suppresses PKR activity and to a lesser degree, PERK activity during ER stress. Our data show that IRE1-SPL axis controls UPR^{mt} activation by impinging on the phosphorylation of eif2α in mammalian cells.

MATERIALS AND METHODS

Reagents and plasmids

Plasmids: SPL (HsCD00378787, Harvard plasmid bank) and FLAG-CMV14 (Addgene). The SPL plasmid was cloned into a FLAG_CMV14 plasmid by restriction and ligation methods.

FLAG_SPL_MUT plasmid is generated from FLAG_ SPL_WT plasmid by using site-directed mutagenesis. IRE1 wildtype (IRE_WT), IRE1 kinase dead (IRE1_KD), and IRE1 analog-sensitive kinase allele (IRE1_ASKA) plasmids are a kind gift from Dr Peter Walter (University of California, San Francisco). Dulbecco's modified Eagle's Medium, phosphate buffer saline (PBS), fetal bovine serum, trypsin, penicillin/ streptomycin (P/S), and L-glutamine were purchased from Thermo Scientific. Protease inhibitor cocktail (P8340), phosphatase inhibitor cocktail-3 (P0044), dimethyl sulfoxide (DMSO; D8418), and doxycycline monohydrate (D1822) were purchased from Sigma. IRE1 kinase inhibitor, KIRA6 (19151), SPL inhibitor [2-acetyl-5-tetrahydroxybutyl imidazole, THI (13222)], and SPL Fluorogenic Substrate (13238) were purchased from Cayman. IRE1 kinase inhibitor, AMG 18 hydrochloride (6166), was purchased from Tocris. The IRE1 RNase inhibitor, 4μ8c (412512), and PERK inhibitor I (516535) were purchased from Calbiochem. Thapsigargin (TG) (sc-24017), tunicamycin (sc-3506), and PKR Inhibitor (sc-204200) were purchased from Santa Cruz Biotechnology. Polyethylenimine (PEI; 23966) was purchased from Polysciences. Primary antibodies: IRE1 phospho-S724 (ab124945; Abcam), IRE1α (3294; Cell Signaling), FLAG (M2) (F1804; Sigma), Human SGPL1 (AF5535; R&D System), Thiophosphate ester antibody [51-8] (ab133473; Abcam), PERK (C33E10) (3192S; Cell Signaling), recombinant PKR (phospho T446) (ab32036; Abcam), PKR (B-10) (sc-6282; Santa Cruz Biotechnology), eIF2 alpha (phospho Ser51)(GTX24837; GeneTex), eIF2α (9722; Cell Signaling), Mortalin/GRP75 (N52A/42) (75–127; Antibodies Incorporated), CLPP (WH0008192M1-100 UG; Sigma), LONP1/Lon (ab103809; Abcam), SQSTM1 / p62 antibody (ab56416; Abcam), Parkin (Prk8) (4211; Cell Signaling), TOM70 (14528-1-AP, Proteintech), Rho GDI (sc-365190, Santa Cruz Biotechnology), normal Rabbit IgG (2729S; Cell Signaling), and normal Mouse IgG (sc-2025; Santa Cruz Biotechnology) β-Actin (sc-47778; Santa Cruz Biotechnology). Secondary antibodies are anti-Mouse (5450-0011; Seracare Life Sciences Inc), anti-Rabbit (5220-0337; Seracare Life Sciences Inc), and mouse anti-goat IgG-HRP (sc-2354; Santa Cruz Biotechnology).

Primers

Hsa_*GAPDH*_F: 5′- GACCACAGTCCATGCCATCACT -3′
Hsa_*GAPDH*_R: 5′- TCCACCACCCTGTTGCTGTAG -3′
Hsa_*XBP1*_F: 5′- TGCTGAGTCCGCAGCAGGTG -3′
Hsa_*XBP1*_R: 5′- GCTGGCAGGCTCTGGGGAAG -3′
Hsa_*HSPA9*_F: 5′- TGGTGAGCGACTTGTTGGAAT -3′
Hsa_*HSPA9*_R: 5′- ATTGGAGGCACGGACAATTTT -3′
Hsa_*HSPE1*_F: 5′- ATGGCAGGACAAGCGTTTAGA -3′
Hsa_*HSPE1*_R: 5′- CCGATCCAACAGCGACTACT -3′
Hsa_*ATF5*_F: 5′- AGGGGACCGCAAGCAAAAG -3′
Hsa_*ATF5*_R: 5′- GCCTTGTAAACCTCGATGAGC -3′
Hsa_*LONP1*_F: 5′- GACGATCCCCGATGTGTTTCC -3′
Hsa_*LONP1*_R: 5′- GGGCGAGACGAACTTTCCTT -3′
Hsa_*ATF4*_F: 5′- CCCTTCACCTTCTTACAACCTC -3′
Hsa_*ATF4*_R: 5′- TGCCCAGCTCTAAACTAAAGGA -3′
Mmu_*Gapdh*_F: 5′- GTGAAGGTCGGTGTGAACG -3′
Mmu_*Gapdh*_R: 5′- GGTCGTTGATGGCAACAATCTC -3′
Mmu_ *Xbp1*_F: 5′- TGAGAACCAGGAGTTAAGAA-CACGC -3′
Mmu_ *Xbp1*_R: 5′- CCTGCACCTGCTGCGGAC -3′
Mmu_ *Hspa9*_F: 5′- ATGGCTGGAATGGCCTTAGC -3′
Mmu_ *Hspa9*_R: 5′- ACCCAAATCAATACCAACCACTG -3′
Mmu_ *Hspe1*_F: 5′- AGTTTCTTCCGCTCTTTGACAG -3′
Mmu_ *Hspe1*_R: 5′- TGCCACCTTTGGTTACAGTTTC -3′

Mmu_ *Atf5*_F: 5′- TGGGCTGGCTCGTAGACTAT -3′
Mmu_ *Atf5*_R: 5′- GTCATCCAATCAGAGAAGCCG -3′
Mmu_ *Clpp*_F: 5′- GCCTTGCCGTGCATTTCTC -3′
Mmu_ *Clpp*_R: 5′- CTCCACCACTATGGGGATGA -3′
Mmu_ *Lonp1*_F: 5′- CTCATGGTGGAGGTTGAGAA TG -3′
Mmu_ *Lonp1*_R: 5′- CAGAGGGTTCAAGGCGATG ATA -3′
Mmu_ *Atf4*_F: 5′- TCGATGCTCTGTTTCGAATG -3′
Mmu_ *Atf4*_R: 5′- AGAATGTAAAGGGGGCAACC -3′
Mmu_ *Ddit3*_F: 5′- CCTAGCTTGGCTGACAGAGG -3′
Mmu_ *Ddit3*_R: 5′- CTGCTCCTTCTCCTTCATGC-3′

Cell culture and transfection

Mouse embryonic fibroblasts (MEFs) from wildtype (WT), IRE1$^{-/-}$, PERK$^{-/-}$, and PKR$^{-/-}$ mice were a kind gift from Dr Gokhan Hotamisligil (Harvard University, T.H. Chan School of Public Health, Boston). MEFs from eif2α S/S (WT) and eif2α A/A (phospho mutant) mice were a kind gift from Dr Mauro Costa-Mattioli (Baylor College of Medicine, Houston). Human embryonic kidney 293 (HEK293) cells were purchased from ATCC. MEF and HEK293 cells were cultured in Dulbecco's modified Eagle's Medium supplemented with 10% fetal bovine serum and 1% L-glutamine in a humidified, 5% CO_2 at 37°C incubator. Upon reaching 60%–80% confluency, cells were transfected with indicated plasmids using PEI in 1:3 DNA:PEI ratio.

Silencer (si) RNA–mediated knock down

HEK293 cells were electroporated with 50 nM siRNA against *IRE1* (SI00605248; Qiagen), 50 nM siRNA against *SGPL1* (SI00057631; Qiagen), or scrambled siRNA (1027281; Qiagen) using a Neon Electroporator (Invitrogen) according to the manufacturer's protocol. HEK293 cells were treated with TG after 48 h transfection.

RNA isolation and analysis

Trisure (Bioline) was used to isolate total RNA from cells and reverse-transcribed using the RevertAid first strand complementary DNA synthesis kit (K1691; Thermo Scientific) according to the manufacturer's protocols and in a polymerase chain reaction (PCR) machine (Bio-Rad). Quantitative reverse transcription PCR (qRT-PCR) reactions were prepared using Power-up-SYBR green (A25742; Applied Biosystems). Quantifications were performed using the $\Delta\Delta$Ct (threshold cycle) method using the following formula: (primer efficiency) − $\Delta\Delta$Ct, where $\Delta\Delta$Ct means ΔCt (target gene) − ΔCt (reference gene). Gene expression levels were normalized relative to GAPDH mRNA in the same cells.

Western blot

Cells were lysed in phospho-lysis buffer (PLB) [50 mM Hepes (pH 7.9), 100 mM sodium chloride, 10 mM EDTA, 10 mM sodium fluoride, 4 mM tetrasodium diphosphate, 1% Triton X-100, 2 mM sodium orthovanadate, 1 mM PMSF (phenylmethylsulfonyl), 1× phosphatase inhibitor mixture, 1× protease inhibitor mixture]. Lysates were cleared by brief centrifugation; protein concentrations were measured with DC assay (Bio-Rad). Upon adding 5X sodium dodecyl sulphate (SDS) loading dye, cell lysates were boiled, and proteins were subjected to SDS/polyacrylamide gel electrophoresis (PAGE)

separation. Following transfer of the proteins on to nitrocellulose membranes, membranes were blocked with 5% milk and incubated with primary and secondary antibodies incubation in Tris-buffered saline containing 0.1% (vol/vol) Tween-20% and 1% (wt/vol) dry milk or bovine serum albumin. Membranes were developed with ECL (RPN2232; Amersham™) and analyzed using the BioRad chemiluminescence imager.

Immunoprecipitation

Total IREl, FLAG (M2), IgG-Rabbit, or IgG-Mouse control antibodies were conjugated overnight with Protein G Magnetic Beads (1614023; Bio-Rad), which were fist blocked by incubating in 2% fatty acid free bovine serum albumin (A-421-10; GoldBio) on a rotator. Conjugated beads were washed with PLB three times and incubated with HEK293 cell lysate overnight on a rotator. Next day, beads were washed with PLB and boiled upon adding 5× SDS loading buffer for 5 min at 95°C. Proteins were then separated by electrophoresis in SDS-PAGE gels for analysis.

In vitro and cell-based kinase assays

In vitro kinase assay. The immunoprecipitated lysates were washed with PLB buffer three times and kinase buffer (20 mM Hepes pH 7.4, 50 mM KoAC, 1 mM $MnCL_2$, 1 mM $MgCl_2$, 1 mM Na_2Mao_4, and 2 mM NaF) once, followed by incubation in kinase reaction mix (kinase buffer with ATPγS-Kinase substrate, ab138911; Abcam) for 30 min at 30°C. EDTA (0.5 M, pH 8.0) (R1021; Thermo Fisher Scientific) was used to stop reaction. P-nitrobenzyl mesylate (PNBM , ab138910; Abcam) was added and incubated for 45 min at 25°C to generate thiophosphate esters on the thiophosphorylated substrates in the in vitro kinase assay, as previously shown (33). Next day, beads were washed with PLB and boiled after adding 5× SDS loading buffer for 5 min at 95°C. Proteins were then separated by electrophoresis in SDS-PAGE gels for analysis.

Cell-based kinase assay. After transfection with indicated plasmids and 300 nM TG treatment for 1 h, HEK293 cells were collected, washed with PBS, and centrifuged at 1000 rpm. Cell pellets were incubated with kinase buffer containing 30 µg/ml digitonin (D141; Sigma Aldrich) and rotated for 10 min at 30°C. After spinning down, cell pellets were incubated with kinase buffer containing 250 µM N6 furfuryl-ATPγS (F008; Biolog Life Science), 100 µM ATP (sc-20240A; Santa Cruz Biotechnology), and 1 mM GTP for 1 h at 30°C. Kinase reaction was stopped by adding PLB containing 20 mM EDTA. Cells were lysed by quick vortexing (5 s intervals) for 10 min. After centrifugation at highest speed for 15 min, PNBM (final concentration of 12.5 mM) was added to the supernatants. Supernatants were filtered with PD-10 columns and washed with PLB to get rid of PNBM. Eluted supernatants were immunoprecipitated using FLAG-M2 antibody-conjugated beads and rotated at 4°C overnight. Next day, beads were washed with PLB and after adding 5X SDS loading buffer, boiled at 95°C for 5 min. Proteins were then separated by electrophoresis in SDS-PAGE gels for analysis.

Proteomics

Sample preparation—in-gel digestion. Samples were separated by SDS-PAGE and stained with Coomassie blue. The bands were cut from the gel and subjected to in-gel digestion with trypsin (PMID: 25278616). Peptides were extracted from the gel pieces by sonication for 15 min, followed by centrifugation and supernatant collection. A solution of 50:50 water: acetonitrile, 1% formic acid (2X the volume of the gel pieces) was added for a second extraction. The samples were again sonicated for 15 min, centrifuged, and the supernatant pooled with the first extract. The pooled supernatants were processed using speed vacuum centrifugation. The samples were dissolved in 10 µl of reconstitution buffer (96:4 water: acetonitrile, 1% formic acid, and analyzed by liquid chromatography with tandem mass spectrometry (LC-MS/MS).

LC-MS/MS. For peptide separation, the UltiMate 3000 RSLC nano LC system (Dionex) fitted with a trapping cartridge (µ-Precolumn C18 PepMap 100, 5 µm, 300 µm i.d. × 5 mm, 100 Å, Thermo Fisher Scientific) and an analytical column (Acclaim PepMap 100 75 µm × 50 cm C18, 3 µm, 100 Å, Thermo Fisher Scientific) was used. The outlet of the analytical column was coupled directly to a QExactive plus (Thermo Fisher Scientific) using the nanoFlex source in positive ion mode. The peptides were introduced into the mass spectrometer (QExactive plus, Thermo Fisher Scientific) via a Pico-Tip Emitter 360 µm OD × 20 µm ID; 10 µm tip (New Objective), and a spray voltage of 2.3 kV was applied. The capillary temperature was set at 320°C. Full-scan MS spectra with mass range 350–1400 m/z were acquired in profile mode in the FT with resolution of 70,000. The filling time was set at maximum of 30 ms with a limitation of 3×10^6 ions. DDA was performed with the resolution of the Orbitrap set to 35,000, with a fill time of 105 ms and a limitation of 2×10^5 ions. Normalized collision energy of 26 was used. The peptide match algorithm was set to 'preferred' and charge exclusion 'unassigned', charge states 1, 5–8 were excluded.

Data processing. Acquired data were processed by IsobarQuant (PMID: 26379230), as search engine Mascot (v2.2.07) was used. Data were searched against Uniprot Homo sapiens proteome database (UP000005640) containing common contaminants, reversed sequences, and the sequences of the proteins of interest. The data were searched with the following modifications: Carbamidomethyl (C; fixed modification), Acetyl (N-term), Phospho (STY), and Oxidation (M) (variable modifications). The mass error tolerance for the full-scan MS spectra was set to 10 ppm and for the MS/MS spectra to 0.02 Da. A maximum of two missed cleavages was allowed. For protein identification, a minimum of two unique peptides with a peptide length of at least seven amino acids and a false discovery rate below 0.01 were required on the peptide and protein level.

Mitochondrial fractionation

Cells were homogenized in ice-cold mitochondria isolation buffer (250 mM sucrose, 1 mM EDTA, 10 mM Hepes; pH 7.4) containing protease and phosphate inhibitor cocktails. Homogenates were run through 27.5 *g* needle four times and centrifuged at 600 *g* for 5 min at 4°C (to eliminate nuclear and intact membranes). Some of the supernatant was kept for examining the whole cell lysates. The rest of the supernatant was centrifuged at 7,000 *g* at 4°C for 10 min. The supernatant was kept in order to examine the cytosolic fraction. Pellets were resuspended with homogenizing buffer and centrifuged at 7,000 *g* at 4°C for 5 min. The supernatant was carefully removed, and the pellet and mitochondrial fraction were dissolved with PLB. Mitochondrial fraction containing

polyvinylidene difluoride membranes were stained with Ponceau S (P7170-1L; Sigma-Aldrich), washed with distilled water, and imaged using BioRad imager.

SPL fluorogenic substrate assay

The SPL fluorogenic substrate assay was performed according to the manufacturer protocol as previously described (34); cell lysates were incubated with sphinganine 1-phosphate analogue, which is converted to an aldehyde by SPL in the presence of 0.25 mM pyrodoxal-5 phosphate. The reactions were incubated at 37°C for 6 hours, and the aldehyde was converted to umbelliferone upon beta elimination at neutral pH. Utilization of the sphinganine 1-phosphate analog by SPL results in the production of umbelliferone, which releases a fluorescent signal that indicates SPL enzymatic activity. Fluorescent signal intensity was measured using a plate reader (excitation at 325 nm and emission at 452 nm).

Lipidomics analysis

Materials. Avanti Polar Lipids, Ceramide/Sphingoid (Cer/Sph) Internal Standard Mixture I.Eppendorf DNA LoBind 2 ml polypropylene microfuge tubes. Methanol, chloroform, dichloromethane, and acetonitrile (Fisher) were of mass spectrometry grade or HPLC grade. The internal standard mixture (Cer/Sph Mixture I) consisted of 25 μm sphingosine (C17 base), sphinganine (C17 base), sphingosine 1-phosphate (C17 base), sphinganine 1- phosphate (C17 base), lactosyl(ß) C12 ceramide, 12:0 sphingomyelin, glucosyl(ß) C12 ceramide, 12:0 ceramide, 12:0 ceramide 1-phosphate, and 25:0 ceramide in ethanol.

Sample preparation. HEK293 cells were gently with iced-cold PBS. Whole cells were pelleted in 2 ml microfuge tubes at 4°C and stored at −80°C until lipid extraction. Mitochondria fractionation has been performed, and mitochondrial fractions were pelleted in 2 ml microfuge tubes at 4°C and stored at −80°C until lipid extraction For lipid extraction, sample tubes were thawed on ice. The internal standards (10 μl) from Cer/Sph Mixture I was added to each tube. Lipid extraction was initiated with the addition of 726 μl of chloroform: methanol:12.1 N hydrochloric acid (HCl) (40:80:1) after which samples were vortexed in an Eppendorf Thermomixer at full speed at 4°C for 15 min. Then, 720 μl of chloroform was added, and samples were vortexed for another 5 min. Finally, 354 μl of 1 N HCl was added, and samples were vortexed for 2 min. Phases were separated by centrifugation for 5 min at 1,000 g at 4°C. The lower phases were collected in a fresh 2 ml tube. An additional 1098 μl of the theoretical lower phase (chloroform: methanol: 1.185 N HCl 86:14:1, v:v:v) was added to the upper phase followed by vortexing and centrifugation at 1,000 g for an additional 5 min. The resultant lower phase was combined with the previously collected lower phase, and the combination was dried using a refrigerated Labconco Centrivap at −4°C under full vacuum (chamber temperature was brought to room temperature prior to opening the lid at the end). The dried samples were analyzed via liquid chromatography tandem mass spectrometry. Samples were resuspended in 100% methanol (LC-MS Optima grade, Fisher) prior to chromatographic separation at ambient temperature on a C8 column (Thermo Hypersil Gold C8 2.1 × 50; 1.9 μm). The mobile phase consisted of a gradient initiated with 10 mM formic acid in water (A) and 10 mM formic acid in acetonitrile/methanol (50:50 v/v) (B) delivered at a flow rate of 0.3 ml/min by a Waters Acquity UPLC. The gradient progressed from 37% to 100% B from 2 to 10 min following injection. A Waters ACQUITY FTN autosampler set at room T injected 1–5 ul of sample extract. For quantitative analysis, the effluent was monitored by a Waters XEVO TQ-S MS/MS via multiple reaction monitoring in positive ion mode. Protonated S1P with a parent-daughter transition of 380.4–264.4 was detected in positive ion mode using a cone voltage of 55 and collision energy of 18. Lipid levels were calculated from peak areas normalized to internal standards. A further normalization was applied based on total protein quantification of the samples.

Mitochondria Ca^{2+} measurements

WT MEF cells were treated with 100 nM TG for indicated time points. RHOD-2 AM (1 μM) (cell-permeable fluorescent calcium indicator) (Thermo Fisher Scientific) was used for mitochondria-specific calcium measurement according to previously published protocols (35).

Mice studies and treatments

Apolipoprotein E-deficient ($Apoe^{-/-}$) mice were purchased from Jackson laboratory. Starting at 8–10 weeks old, $Apoe^{-/-}$ mice were fed with high cholesterol/high fat atherosclerotic mouse diet from Envigo (TD.88137) for 12 weeks. $Apoe^{-/-}$ mice received intraperitoneal injections of either AMG18 (30 mg/kg) or vehicle twice per day in final 4 weeks of diet, both delivered in 20% vol/vol cremophor-EL (Sigma) saline solution.

Study approval

All animal experiments were performed according to protocols approved by the Experimental Animal Ethical Care Committees at Cedars Sinai Medical Center, Los Angeles, USA.

Statistical analysis

In vitro experiments were analyzed with either unpaired t test with Welch's correction. Figures analyzed by unpaired t test are mentioned in related figure legend. Mann-Whitney was used for in vivo experiments. (Mean as center value, two-tailed, *$P \leq 0.05$, **$P \leq 0.01$, ***$P \leq 0.001$, ****$P \leq 0.0001$).

RESULTS

ER stress induces UPR^{mt} in an IRE1 kinase-dependent manner

Past studies have shown that chronic ER stress induces mitochondrial proteases that play a critical role in the execution of UPR^{mt}; however, whether ER stress can induce full-fledged UPR^{mt} signaling has not been examined before (28, 36). To approach this, we treated mouse fibroblasts with TG, which is a ER toxin that inhibits the ER calcium ATPase (4). TG simultaneously induced UPR^{ER} and UPR^{mt} in wildtype (WT or IRE1$^{+/+}$) MEFs as evident by the induction of key transcription factors for both stress responses such as ATF4, CHOP, and ATF5 (that are encoded by *Atf4*, *Ddit3*, and *Atf5*, respectively), mitochondrial chaperons such as mtHSP70 and HSP10 (that are encoded by *Hspa9* and *Hspe1*, respectively), and mitochondrial proteases such

as LONP1 and CLPP1 (that are encoded by *Lonp1* and *Clpp*, respectively) (**Fig. 1**A–F). Tunicamycin, another ER toxin that inhibits protein glycosylation (4) also led to robust induction of both UPR^{ER} and UPR^{mt} in WT MEFs (supplemental Fig. S1A). Moreover, both ER toxins were able to induce UPR^{mt} in human cells (HEK293 cells) (supplemental Fig. S1B, C). However, IRE1-deficiency (IRE1$^{-/-}$) prevented ER stress from inducing UPR^{mt} signaling (Fig. 1A–F). Collectively, these findings demonstrate that ER stressors can induce UPR^{mt} signaling in an IRE1-dependent manner.

IRE1 harbors dual enzymatic activities in its kinase and endoribonuclease domains (4). We next asked which of the two IRE1 enzymatic activities is required for UPR^{mt} induction during ER stress. Inhibition of IRE1 kinase domain with two different, specific inhibitors, namely KIRA6 and AMG18, (37–39) blocked TG from inducing robust UPR^{mt} signaling in WT MEF cells (**Fig. 2**A–K). Moreover, blocking IRE1 kinase domain activity in vivo by AMG18 reduced the level of UPR^{mt} markers in the livers from hyperlipidemic mice (supplemental Fig. S2A–E). Conversely, IRE1 RNase-
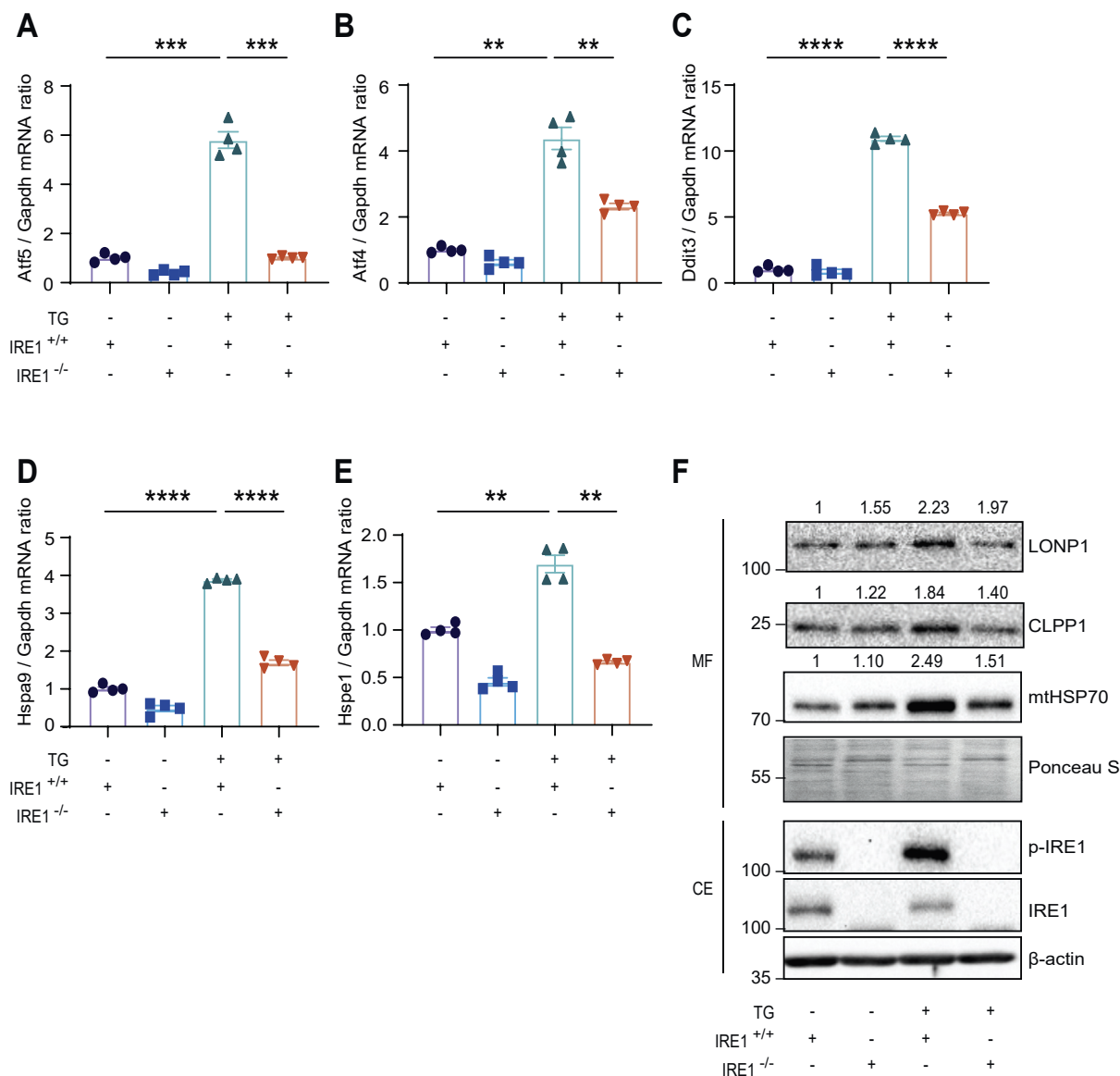
Fig. 1. IRE1-deficiency blocks UPR^{mt} induction during ER stress. A–E: IRE1$^{+/+}$ and IRE1$^{-/-}$ MEFs were treated with TG (100 nM; 12 h), and total RNA was analyzed by qRT-PCR for Atf5, Atf4, Ddit3, Hspa9, Hspe1, and Gapdh mRNA (n = 4 biological replicates). F: IRE1$^{+/+}$ and IRE1$^{-/-}$ MEFs were treated with TG (100 nM; 4 h) and mitochondrial fraction (MF) and total cellular extract (CE) protein lysates were analyzed by Western blotting using specific antibodies for LONP1, mtHSP70, CLPP1 (for MF) and p-IRE1, IRE1 and β-actin (for CE). The membrane was stained by Ponceau S (n = 3 biological replicates; a representative blot is shown). Data information: All data are mean ± SEM; (n = 4). Unpaired *t* test with Welch's correction. * $P \leq 0.05$, ** $P \leq 0.01$, *** $P \leq 0.001$, **** $P \leq 0.0001$. ATF, activating transcription factor; CLPP1, caseinolytic protease-1; ER, endoplasmic reticulum; IRE1, inositol-requiring enzyme-1; LONP1, Lon protease-1; MEFs, mouse embryonic fibroblasts; mtHSP70, mitochondrial heat shock protein 70; mt, mitochondria; TG, thapsigargin; UPR, unfolded protein response.
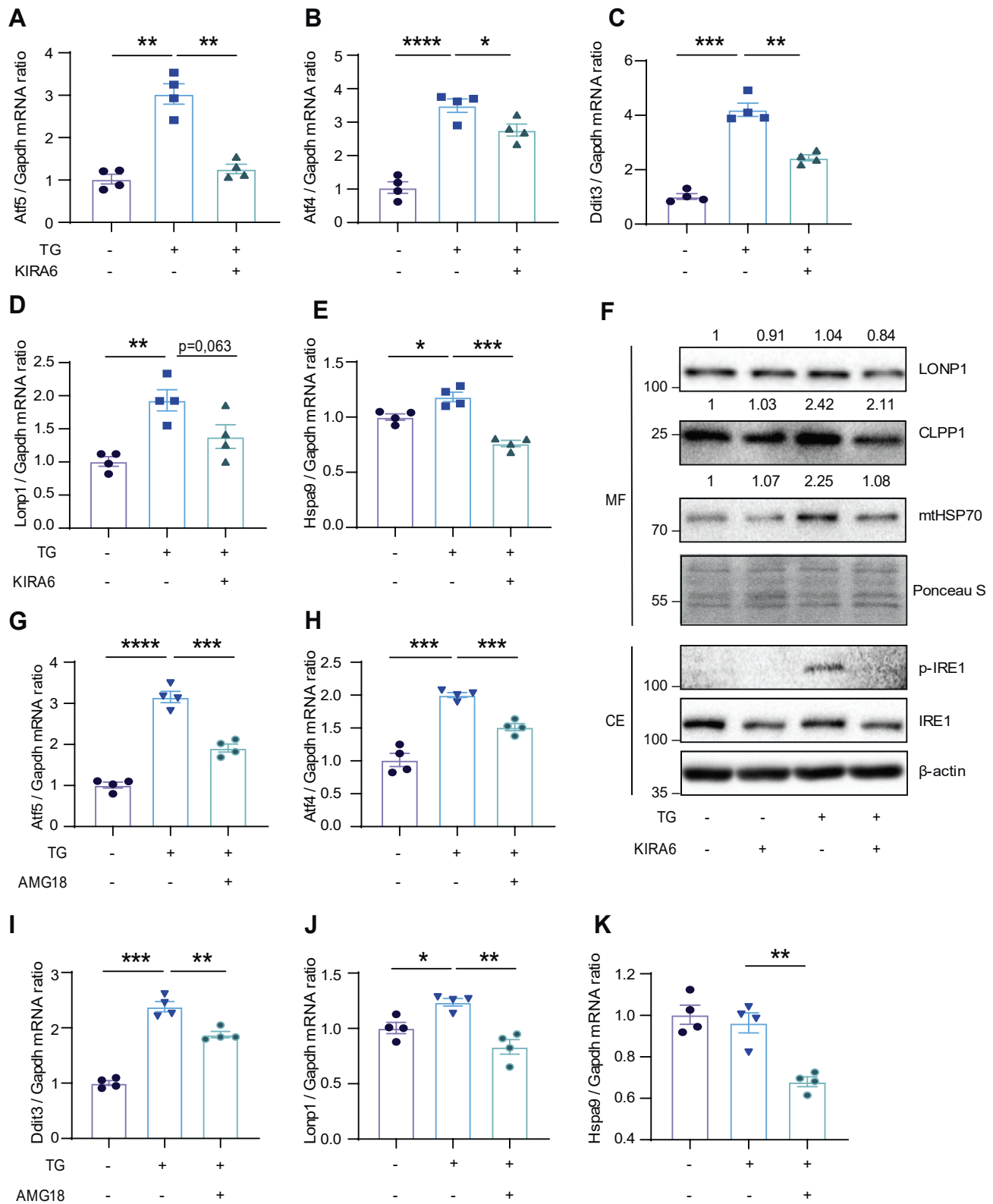
Fig. 2. ER stress induces UPR^{mt} in an IRE1 kinase-dependent manner. A–E: Wild type (WT) MEFs were treated with KIRA6 (5 μM) and TG (100 nM) for 12 h, and total RNA was analyzed by qRT-PCR for Atf5, Atf4, Ddit3, Lonp1, Hspa9, and Gapdh mRNA (n = 4 biological replicates). F: WT MEFs were treated with KIRA6 (5 μM) and TG (100 nM) for 4 h, and MF and CE protein lysates were analyzed by Western blotting using specific antibodies against LONPl, mtHSP70, and CLPP (for MF) and p-IRE1, total IRE1, and β-actin (for CE). The membrane was stained by Ponceau S (n = 3 biological replicates; a representative blot is shown). G–K: WT MEFs were treated with 2 μM AMG18 and 100 nM TG for 12 h, and total RNA was analyzed by qRT-PCR for Atf5, Atf4, Ddit3, Lonpl, Hspa9, and Gapdh mRNA (n = 4 biological replicates). Data information: All data are mean ± SEM; (n = 4). Unpaired t test with Welch's correction. * $P \le 0.05$, ** $P \le 0.01$, *** $P \le 0.001$, **** $P \le 0.0001$. ATF, activating transcription factor; CE, total cellular extract;

specific inhibitor, 4μ8c (40) did not prevent TG-induced ATF4, CHOP, LONPl, CLPPl, and mtHSP70 despite effectively inhibiting specific IRE1 RNase domain substrate, Xbp1 mRNA (supplemental Fig. S3A–G). All together, these data show that IRE1 kinase activity, and not its RNase activity, plays a key role in robust activation of UPR^{mt} by ER stress.

ER stress–induced IRE1 phosphorylates SPL

While IRE1 RNase activity, its substrates and downstream actions in the UPR^{ER} are well characterized, IRE1's kinase activity and substrate(s) are not (4). Recently published mass spectrometry–based IRE1 interactome data revealed that IRE1 potentially interacts with SPL (30, 41). SPL enzyme degrades S1P irreversibly, and this reaction is referred as the exit point of sphingolipid metabolism. S1P is a signaling lipid found in very small quantities, and its level is transiently and strictly controlled by specific S1P kinases and phosphatases in addition to SPL (31). The ablation of SPL activity can significantly increase cellular levels of S1P and have considerable biological impact. Recent studies highlight the importance of S1P for mitochondria-related pathways. S1P has been shown to bind to mitochondrial prohibitin 2 (PHB2) protein to regulate the activity of mitochondrial respiratory complexes which are crucial for sustaining mitochondrial health (42). Moreover, SPL deficiency has been shown to associate with impaired mitochondrial function and morphology (43). A study in nematodes show that mitochondrial stress can promote the phosphorylation of sphingosine to yield S1P, resulting in potent UPR^{mt} signaling. In the same study, SPL knockdown potentiates UPR^{mt} under mitochondrial stress conditions (32). However, the contribution of SPL in UPR^{mt} signaling in mammalian cells is not known. Here, we asked whether IRE1 interaction with SPL modifies S1P-induced UPR^{mt} in mammalian cells undergoing ER stress.

First, we sought to experimentally validate the possible physical interaction between IRE1 and SPL occurs in mammalian cells as it is predicted by IRE1 interactome data (30, 41). SPL and IRE1 plasmids were cotransfected into cells in which ER stress was induced by TG treatment. The results of this experiment confirmed that IRE1 and SPL interact with each other under both nonstress and stress conditions in cells (Fig. 3A).

Next, we asked whether IRE1 can phosphorylate SPL. WT (IRE1_WT), kinase dead mutant (IRE1_KD; serine 599 mutated to an alanine), and FLAG-tagged SPL (FLAG_SPL) were immunoprecipitated from HEK293 cells that overexpressed these proteins. The

immunoprecipitated IRE1 (kinase) and SPL (substrate) from these cell lysates were incubated in an in vitro kinase assay as previously described. In this reaction, the kinase transferred a thiophosphate group from the provided ATPγS in the kinase buffer onto its substrate. The transferred thiophosphate was further converted to a thio-phosphate ester through an alkylation reaction as described before (33). A thio-phosphate ester-specific antibody was used to detect the thio-phosphorylated IRE1 and SPL by Western blotting. The results of this experiment showed that IRE1_WT phosphorylated SPL in vitro. On the other hand, IRE1_KD could not phosphorylate SPL (Fig. 3B). We next performed a 'cell-based' kinase assay by using a previously characterized ATP analog sensitive kinase allele of IRE1 (IRE1_-ASKA). In this IRE1 mutant, a point mutation in a gatekeeper amino acid in the ATP binding cavity leads to slight enlargement of the cavity sufficient to accommodate an ATP analog with a bulky side chain such as N6 furfuryl-ATPγS. This bulky ATP analog is preferentially used by IRE1_ASKA and not IRE1-WT or IRE1-KD (44, 45). Cells were cotransfected with FLAG_SPL_WT and IRE1_ASKA, IRE1_WT, or IRE1_KD plasmids before inducing ER stress with TG. The kinase assay (using N6 furfuryl-ATPγS) result shows that IRE1_ASKA efficiently phosphorylated SPL inside the cells but not IRE1_WT or IRE1_KD (Fig. 3C).

To discover which amino acids on SPL are phosphorylated by IRE1, an in vitro kinase assay (using ATP in the kinase buffer) was set up with SPL (as substrate) in the presence or absence of IRE1_WT (as kinase). The mass spectroscopy–based, phospho-proteomics analysis that followed the kinase reaction revealed that serine 286 (S286) and threonine 287 (T287) on SPL are phosphorylated by IRE1 kinase (supplemental Fig. S4). Of note, both IRE1-targeted amino acids and their neighboring amino acid sequences on SPL are highly conserved across the species (Fig. 3D). Next, we mutated T287 on SPL to alanine (SPL_MUT), which cannot be phosphorylated. We observed that IRE1 could no longer phosphorylate the SPL_MUT in an in vitro kinase assay, demonstrating T287 is an IRE1-dependent phosphorylation site on SPL (Fig. 3E).

IRE1 kinase inhibits SPL activity and induces S1P levels during ER stress

What is the consequence of SPL phosphorylation by IRE1 on SPL's enzymatic activity? S1P, produced by sphingosine kinases 1 and 2 (SPHK1 and SPHK2), is irreversibly degraded by SPL (Fig. 4A) (31). SPL activity can be measured from cell lysate by incubating with a fluorogenic substrate in a SPL activity assay as previously described (34). The induction in the fluorogenic

---

CLPPl, caseinolytic protease-l; ER, endoplasmic reticulum; IRE1, inositol-requiring enzyme-l; MEFs, mouse embryonic fibroblasts; MF, mitochondrial fraction; mt, mitochondria; mtHSP70, mitochondrial heat shock protein 70; LONPl, Lon protease-l; TG, thapsigargin; UPR, unfolded protein response.
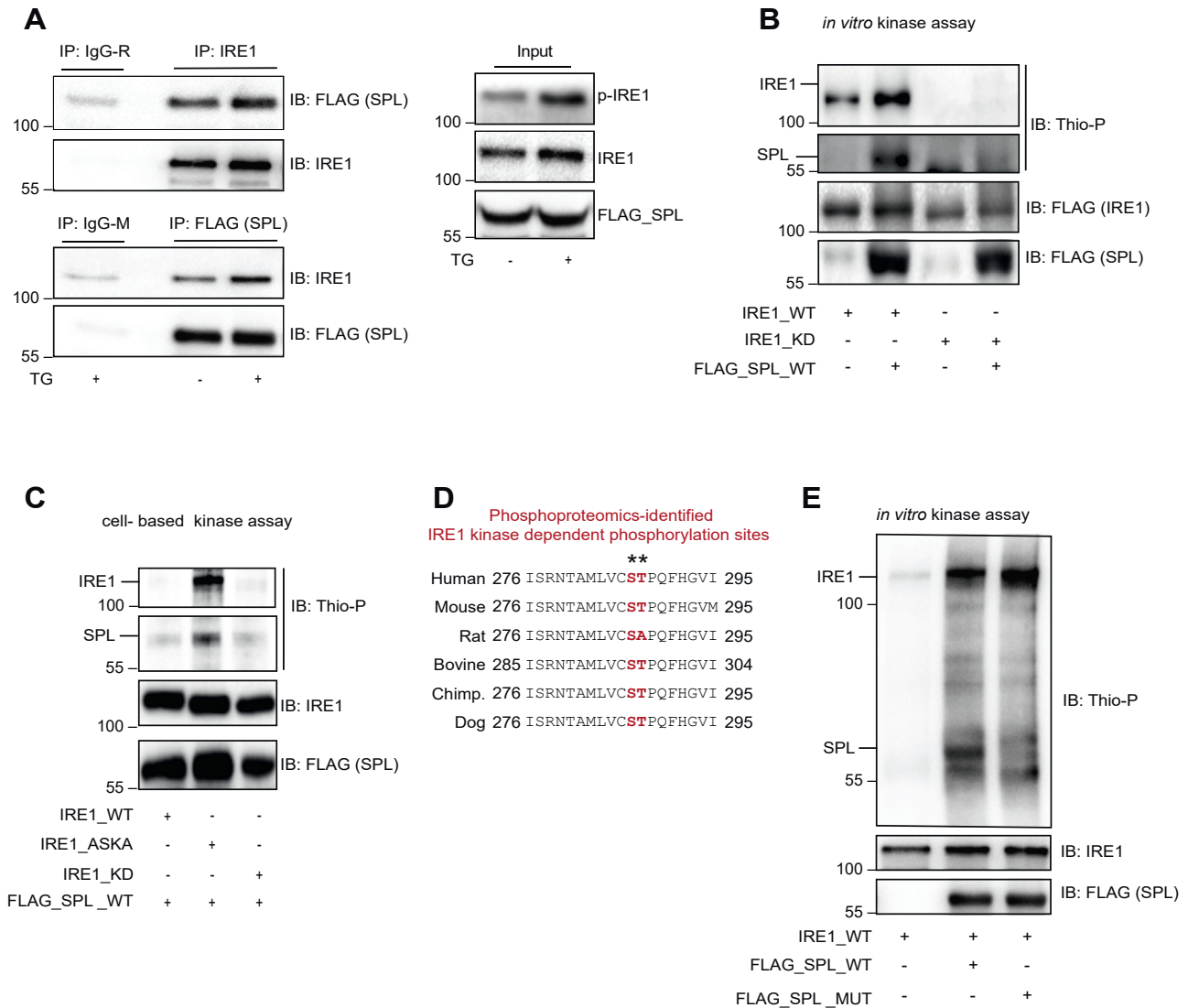
Fig. 3. IRE1 phosphorylates SPL during ER stress. A: HEK293 cell were cotransfected with IRE1 and FLAG-SPL plasmids and treated with TG (600 nM; 4 h). IRE1 and SPL were immunoprecipitated with total IRE1 and FLAG antibodies, respectively, and analyzed by Western blotting using antibodies specific for total IRE1 and FLAG. Normal IgG Rabbit or normal IgG-Mouse antibodies were used to show specify of IRE1 and FLAG antibodies, respectively. The cell lysate was also analyzed by Western blotting using antibodies specific for p-IRE1, total IRE1, and FLAG (n = 4 biological replicates, a representative blot is shown). B: *In vitro* kinase assay: HEK293 cells were transfected with the indicated plasmids and treated with TG (1 μM; 2 h). IRE1 and SPL were immunoprecipitated with FLAG antibodies and incubated together with ATPγS in a kinase reaction. The kinase reaction was analyzed by Western blotting using specific antibodies for thio-phospho ester and FLAG (n = 3 biological replicates, a representative blot is shown). C: "Cell-based" kinase assay: HEK293 cells were transfected with the indicated plasmids and treated with TG (1 μM; 2 h) followed by treatment with N6 furfuryl-ATPγS. Immunoprecipitated lysates were analyzed by Western blotting with specific antibodies for thio-phospho ester, total IRE1, and FLAG (n = 3 biological replicates; a representative blot is shown). D: Multiple amino acid sequence alignment of SPL from different species: * indicates possible IRE1-mediated phosphorylation sites as determined by mass spectrometry. E: *In vitro* kinase assay: HEK293 cells were transfected with the indicated plasmids and treated with TG (1 μM; 2 h). IRE1 and SPL were immunoprecipitated with total IRE1 and FLAG antibodies, respectively, and incubated together with ATPγS in a kinase reaction. The kinase reaction was analyzed by Western blotting using specific antibodies for thio-phospho ester, total IRE1 and FLAG (n = 3; a representative blot is shown). ER, endoplasmic reticulum; HEK293, human embryonic kidney 293; IRE1, inositol-requiring enzyme-1; SPL, sphingosine 1-phosphate lyase; TG, thapsigargin.

signal (upon conversion of sphinganine 1-phosphate to umbelliferone) in the assay indicates SPL activity. We observed that TG treatment led to the inhibition of SPL activity in this assay, consistent with a previous study that showed ER stress induces cellular S1P levels (Fig. 4B). (46). Furthermore, the inhibition of SPL

activity by TG was reversed by the IRE1 kinase inhibitors (KIRA6 and AMG18), but not by the IRE1 RNase inhibitor (4μ8c) (Fig 4B–C). TG further inhibited SPL activity when IRE1_WT was cotransfected with SPL_WT, showing that SPL activity is sensitive to TG-induced IRE1 activity (Fig. 4D). In contrast, TG has no
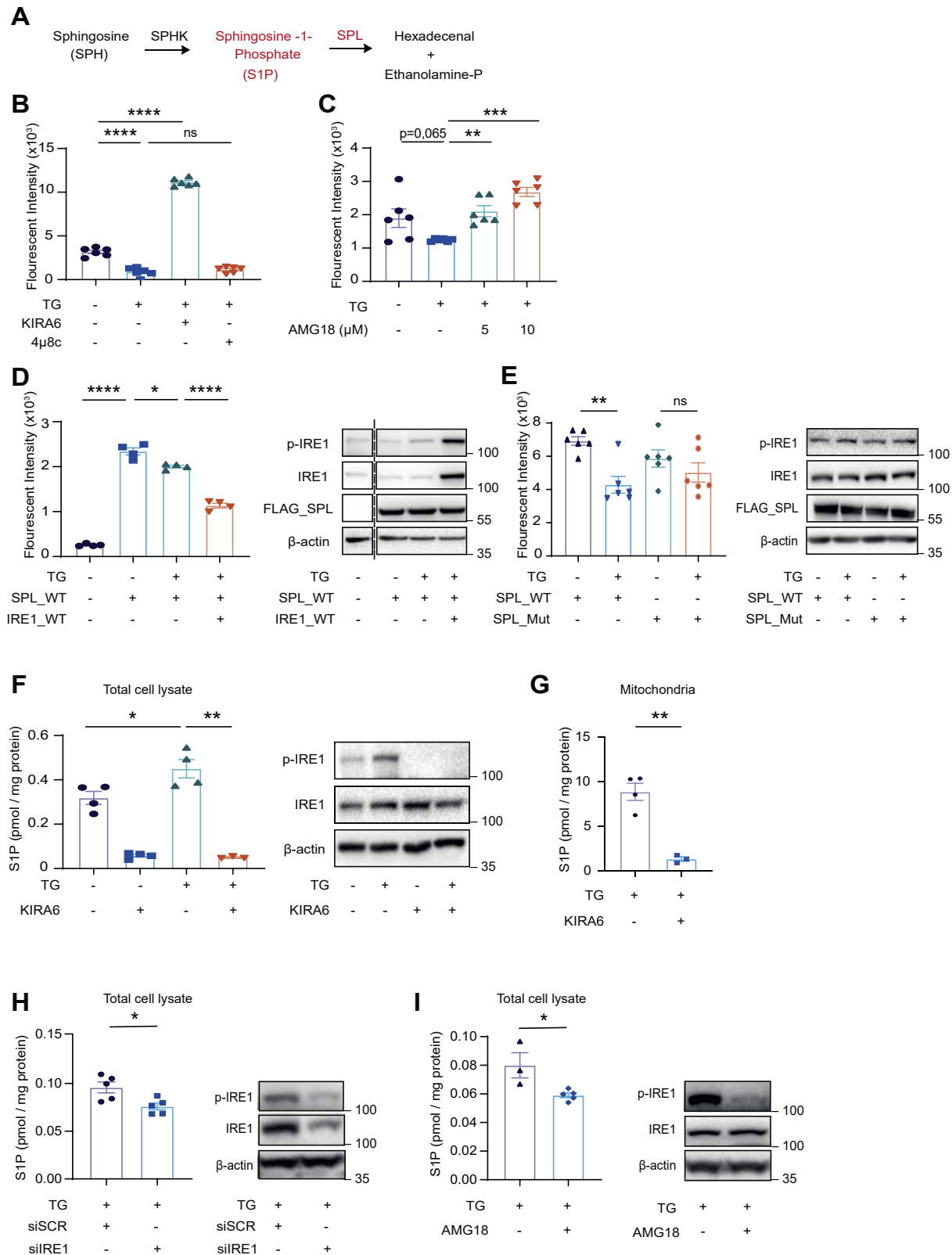
Fig. 4. ER stress suppresses SPL activity and induces cellular S1P levels. A: S1P degradation by SPL activity. B–E: SPL fluorogenic substrate assay was performed according to the manufacturer protocol on the cellular lysates from: (B) HEK293 cells that were treated with KIRA6 (20 μM) or 4μ8c (100 μM) and TG (600 nM; 2 h) (n = 6 biological replicates); C: HEK293 cells were that were treated with AMG18 (5–10 μM) and TG (600 nM; 2 h) (n = 6 biological replicates); and D–E: HEK293 cells that were transfected with the indicated plasmids and treated with TG (600 nM; 2 h) (n = 4 biological replicates for D and n = 6 biological replicates for E). F–I: lipid quantification was performed by LC-MS/MS from lysates of HEK293 that were (F–G) pretreated with KIRA6 (20 μM; 1 h) and then treated with TG (600 nM) or vehicle for 2 h (n = 4 biological replicates for DMSO, KIRA6, and TG, n = 3 biological replicates for KIRA6+TG), S1P is measured from total cell lysates (F) and from isolated mitochondria (G, H) transfected with scrambled (siSCR)

≋ASBMB

effect on the activity of SPL_MUT, showing IRE1-dependent SPL phosphorylation (on T287) is critical for inhibition of SPL activity by ER stress (Fig. 4E).

It has been shown that SPL deficiency or inhibition leads to the accumulation of S1P in cells (47, 48). Using LC-MS, we next assessed changes in S1P levels during ER stress. Acute ER stress (induced by 2 h of TG treatment) resulted in a significant increase in intracellular S1P level (Fig. 4F), consistent with a previous report that showed ER stress leads to S1P accumulation in cells (46). The results of our SPL activity assay had shown that IRE1 kinase inhibitor, KIRA6, prevents TG-induced SPL activity suppression (Fig. 4B). Consistent with this, IRE1 kinase inhibitor prevented TG-induced S1P accumulation (Fig. 4F). These results show that increase in S1P levels upon ER stress is dependent on IRE1's kinase activity. KIRA6 is a potent inhibitor that completely diminishes both basal and TG-induced IRE1 kinase activity (Fig. 4F). KIRA6 induces SPL activity in nonstress and TG-treated stress conditions (higher than that of basal SPL activity level in nonstressed cells) while reducing S1P levels in parallel (supplemental Fig. S5A and Fig. 4F), suggesting that the IRE1 kinase-induced SPL phosphorylation also plays a role in maintaining the basal level of S1P in nonstressed cells. Moreover, inhibition of IRE1 kinase domain by KIRA6 also significantly reduced mitochondrial S1P accumulation during ER stress (Figs. 4G and S5B). To further confirm the effect of IRE1 on cellular S1P levels under stress conditions, we knocked down IRE1 expression by a specific siRNA and used a second IRE1 kinase inhibitor, AMG18. These treatments had partial but strong inhibitory effect on TG-induced IRE1 kinase (as assessed by its autophosphorylation in Fig. 4H–I). Both IRE1 knockdown and AMG18 also reduced intracellular S1P levels under ER stress condition (Fig. 4H–I). Collectively, these results demonstrate that suppression of IRE1 kinase can prevent ER stress-induced accumulation of intracellular S1P (Fig. 4F–I) simultaneous to UPR^mt induction (Figs. 1 and 2).

IRE1-SPL axis potentiates UPR^mt

In *C.elegans*, mitochondrial stress–induced SPHK1 translocation to the outer mitochondrial membrane results in increased S1P production that initiates UPR^mt activation (32). We aimed to investigate whether SPL has any impact on UPR^mt activation in mammalian cells. SPL_WT overexpression resulted in significantly higher SPL activity in cells (**Fig. 5**A) while blocking ER stress–induced UPR^mt signaling by the inhibition of

TG-induced p-eiF2α, ATF4, CHOP, ATF5, mtHSP70, LONP1, and CLPP1 (**Fig. 5**B–G) We next used a SPL-specific inhibitor (THI) to inhibit cellular SPL activity. THI treatment significantly enhanced TG-induced UPR^mt signaling (**Fig. 6**A–F). These results show that SPL activity is critical for ER stress–induced UPR^mt signaling.

To address the role of IRE1-mediated SPL phosphorylation in ER stress-induced UPR^mt signaling, we next examined the impact of SPL_MUT, which does not get phosphorylated by IRE1, on UPR^mt signaling during ER stress. Whereas SPL_WT overexpression resulted in significant reduction in ER stress–induced UPR^mt signaling, this effect was diminished when IRE1-mediated phosphorylation site was mutated on SPL (Fig. 6G–J). This result supports that IRE1-dependent SPL phosphorylation plays a critical role in UPR^mt regulation.

We next asked how IRE1- SPL axis regulates UPR^mt signaling. Since mammalian UPR^mt requires eif2α phosphorylation, we investigated whether IRE1 deficiency had any impact on the activation of eif2α kinases (17). Intriguingly, IRE1 knockdown with a specific siRNA or inhibition of its kinase activity both prevented TG-induced eif2α phosphorylation (**Figs. 7**A and S6A). ER stress is known to induce only two of the eif2α kinases, namely PERK and PKR (49–52). Indeed, IRE1 knockdown led to a profound inhibition of TG-induced PKR phosphorylation while only partially reducing TG-induced PERK phosphorylation (Fig. 7A). In a parallel experiment, SPL_WT overexpression also completely abrogated PKR phosphorylation and partially reduced PERK phosphorylation while simultaneously preventing eif2α phosphorylation during ER stress (Fig. 7B). As expected, SPL knock down with a specific siRNA led to a profound induction in PKR autophosphorylation and to a lesser degree in PERK phosphorylation while simultaneously inducing downstream eif2α phosphorylation during ER stress condition (Fig. 7C).

We also assessed the roles PKR and PERK in ER stress-induced activation of UPR^mt. PKR- and PERK-deficient MEFs both displayed marked disruption in ER stress-induced UPR^mt activation (Fig. 7D–F). In addition, the inhibition of both PKR and PERK with their specific inhibitors also abrogated ER-stress induced UPR^mt induction (supplemental Fig. S6B–E). As shown earlier, inhibition of SPL by its specific inhibitor, THI, augments TG-induced UPR^mt signaling (Fig. 6A–F). However, THI could not enhance
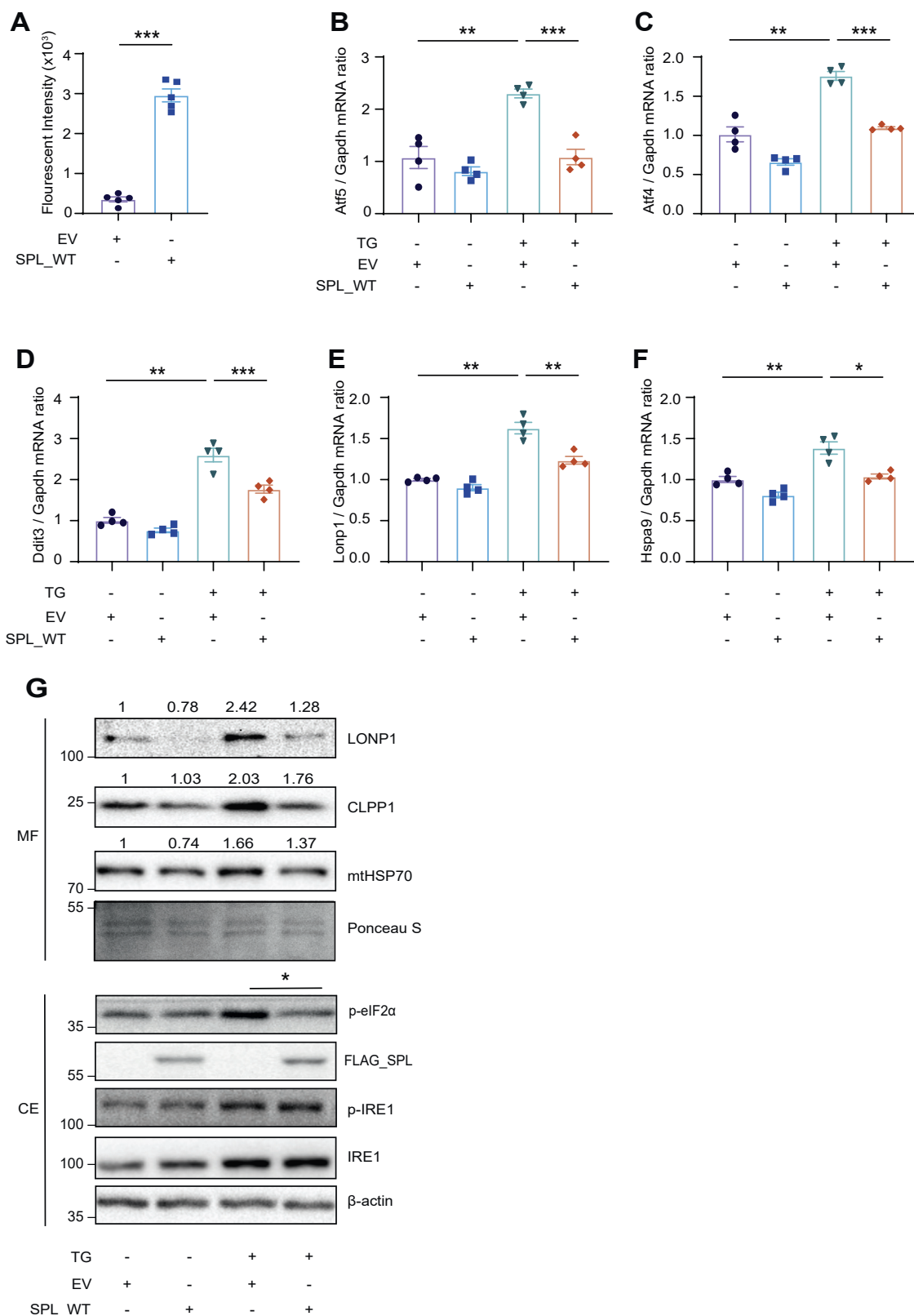
Fig. 5. SPL overexpression reduces ER stress–induced UPR[mt]. A: HEK293 cells were transfected with either empty vector (EV) or SPL_WT plasmid, and the cell lysates were used to perform the SPL fluorogenic substrate assay according to manufacturer's protocol (n = 5 biological replicates). B–F: WT MEFs were transfected with either EV or SPL_WT and treated with TG (100 nM; 12 h). Total RNA was analyzed by qRT-PCR for Atf5, Atf4, Ddit3, Lonp1, Hspa9, and Gapdh mRNA (n = 4 biological replicates). G: WT MEFs were transfected with the indicated plasmids and treated with TG (100 nM; 4 h). MF protein lysates were analyzed by Western blotting using specific antibodies for LONP1, mtHSP70, and CLPP1 and CE protein lysates with antibodies for p-IRE1, IRE1, FLAG, p-eif2α, and β-actin. The membrane was stained with Ponceau S. (n = 3 biological replicates; a representative blot is shown). Data

TG-induced UPR^{mt} in PKR- or PERK-deficient MEFs like it did in the WT MEFs (Fig. 7D–F).

To further validate our hypothesis, we treated MEFs from mice that have wild type eif2α (or eif2α S/S to indicate serine on 51st amino acid) or a phosphorylation mutant of eif2α (or eif2α A/A to indicate alanine on the 51st amino acid) with the SPL inhibitor, THI. Inhibition of SPL by THI enhanced the transcription of TG-induced ATF4 and ATF5 in eif2α S/S MEFs but not in the eif2α A/A MEFs (supplemental Fig. S6F–H). Next, we transfected eif2α S/S and eif2α A/A MEFs with either SPL_WT or SPL_MUT and induced ER stress. Consistent with our previous results, SPL overexpression significantly reduced UPR^{mt} signaling in eif2α S/S MEFs upon ER stress conditions, but this effect was diminished when SPL_MUT was transfected into the same type of WT cells. Neither SPL_WT nor SPL_MUT had an effect on UPR^{mt} signaling in ER stressed eif2α A/A MEFs (Figs. 7G–I and S6I). Collectively, these data demonstrate IRE1-SPL axis impinges on eif2α phosphorylation to induce a robust UPR^{mt} signaling during ER stress in mammalian cells (Fig. 8).

UPR^{mt} induction is unlikely to be due to an increase in Ca^{2+} transfer between the organelles

We wanted to gain more insight into how IRE1 prevents ER stress–induced UPR^{mt} in our experimental system. Several studies have shown that both IRE1 and PERK can localize to mitochondria-associated ER membranes and modulate calcium homeostasis (53, 54). Ca^{2+} uptake in the ER is mediated by the sarcoreticulum and endoplasmic reticulum Ca^{2+}-ATPase (SERCA) family of pumps, which are inhibited by TG. TG treatment (10 μM or higher) leads to an acute rise in intracellular Ca^{2+} and increased Ca^{2+} influx into the mitochondria, resulting in mitochondrial respiration defect (55). IRE1 deficiency has been shown to significantly reduce mitochondrial Ca^{2+} uptake (53). In our study, the low doses of TG used to activate IRE1 kinase activity did not increase intramitochondrial Ca^{2+} but was sufficient to induce UPR^{mt} (supplemental Fig. S8). ER stress–induced Ca^{2+} transfer to the mitochondria is unlikely to contribute to UPR^{mt} induction in our experimental design.

Inhibition of IRE1-SPL axis is consistent with enhanced mitophagy

ER stress-induced phosphorylation of eif2α by PERK plays a critical role in transcriptional and translation induction of LONP1 (28). LONP1 is a key mitochondrial protease that degrades unfolded proteins during UPR^{mt} signaling and inhibits mitophagy through degrading the mitophagy regulator, Phosphatase and tensin homolog-induced kinase 1 (15). It is not clear how UPR^{ER} communicates these two divergent fates to the mitochondria. Because ER stress is unable to induce LONP1 protein level when IRE1 kinase is inhibited (Fig 2D, F), suppression of UPR^{mt} signaling by IRE1 kinase inhibitor would be predicted to promote mitophagy. Indeed, we found that both IRE1 kinase inhibition (supplemental Fig. S9A) and SPL overexpression (supplemental Fig. S9B) in ER-stressed cells can induce the recruitment of p62 adaptor protein and Parkin E3 ubiquitin ligase to the mitochondria, a result that is consistent with enhanced mitophagy.

DISCUSSION

Organisms evolved various mechanisms to sense organelle dysfunction and to restore homeostasis in subcellular compartments such as the ER and mitochondria. The ultimate goal of these mechanisms is to regain cellular health by salvaging organelles or clearing those that are beyond repair. Less understood is how the decision for salvation versus clearance of organelles is made in mammalian cells. Chronic organelle stress is intertwined with pathological situations such as obesity, diabetes, and atherosclerosis (24). Due to functional overlap and physical association between ER and mitochondria, unresolved stress in one of these organelles can spread to the other. ER stress induced by unfolded proteins or lipid bilayer stress can also lead to mitochondrial dysfunction, mitochondrial oxidative stress, and trigger inflammation (28, 40, 56). Several mechanisms couple ER stress to mitochondrial dysfunction, including enhanced ER-to-mitochondria calcium transfer and PERK-induced mitophagy inhibition (28). Conversely, mitochondria dysfunction can spread to the ER. For example, mitochondrial translation inhibitor, doxycycline, or mitochondrial toxin, paraquat, induce not only UPR^{mt} but also UPR^{ER} signaling in mouse and human cells in published studies (29, 57) as well as in our own data. Our findings in this study reveal that during ER stress, IRE1 phosphorylates SPL to induce intracellular S1P leading to the activation of UPR^{mt} that is conserved from nematodes to humans (32).

An important revelation in this study has been that IRE1's kinase activity is required for UPR^{mt} induction during ER stress. IRE1's RNase activity is known for its essential role in UPR^{ER} activation, but our data exclude it from playing a role in UPR^{mt} signaling. This striking uncoupling of IRE1's kinase and RNase functions in UPR^{ER} and UPR^{mt} led us to the discover a new
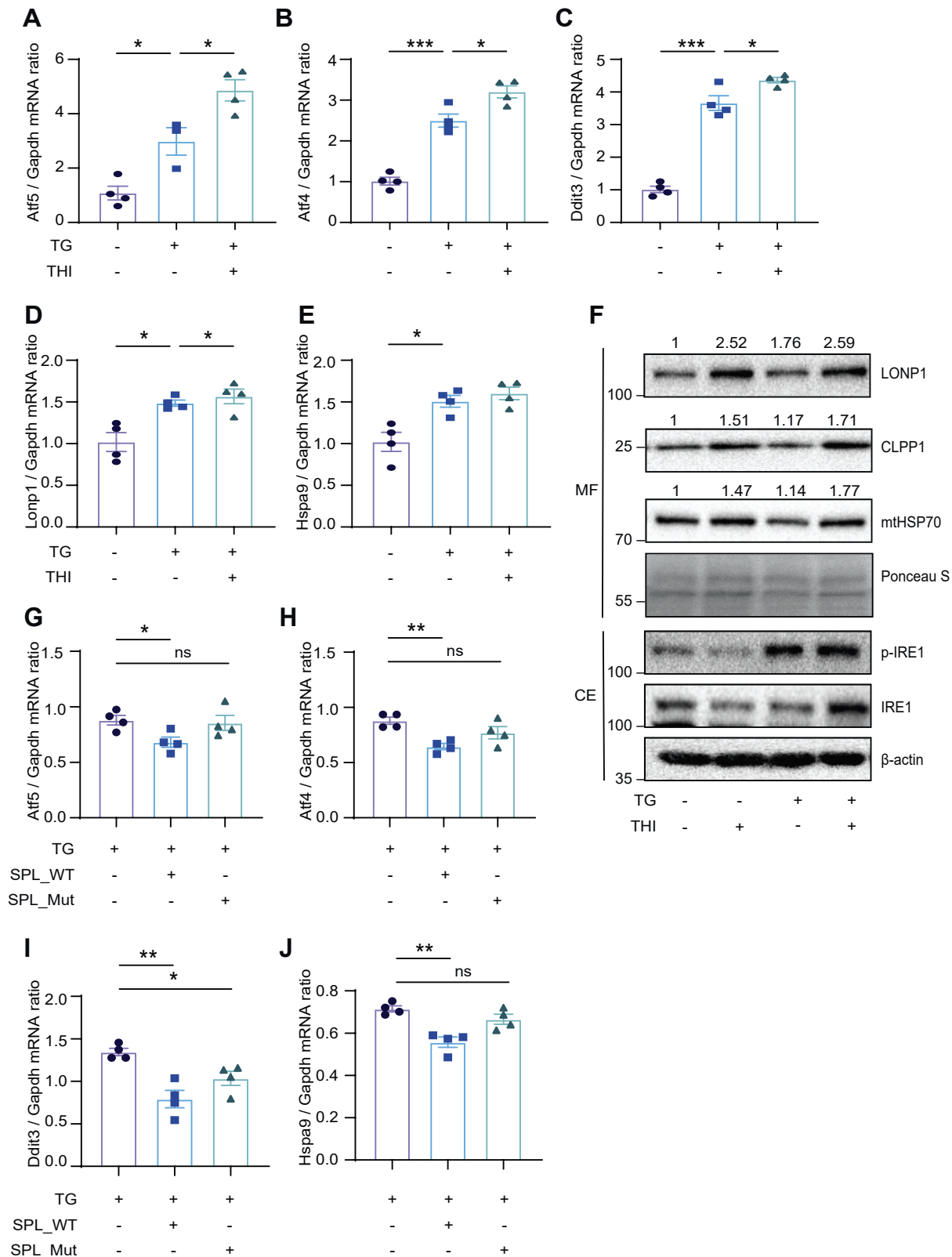
Fig. 6. IRE1-SPL signaling axis augments UPR^{mt}. A–E: WT MEFs were treated with THI (5 mM) and TG (100 nM) for 12 h, and total RNA lysate was analyzed by qRT-PCR for Atf5, Atf4, Ddit3, Lonp1, Hspa9, and Gapdh mRNA (n = 4 biological replicates). F: WT MEFs were treated with THI (5 mM) and TG (100 nM) for 4 h, and MF protein lysates were analyzed by Western blotting using specific antibodies for LONP1, mtHSP70, and CLPP1 and CE protein lysates with antibodies for p-IRE1, IRE1, and β-actin. Ponceau S was used as loading control. (n = 3 biological replicates; a representative blot is shown). G–J: WT MEFs were transfected with the indicated plasmids and treated with TG (100 nM: 20 h). Total RNA lysate was analyzed by qRT-PCR for Atf5, Atf4, Ddit3, Hspa9, and Gapdh mRNA (n = 4 biological replicates). Data information: All data are mean ± SEM; (n = 4) Unpaired t test with Welch's correction. * $P \leq 0.05$, ** $P \leq 0.01$, *** $P \leq 0.001$. ATF, activating transcription factor; CE, total cellular extract; CLPP1, caseinolytic

substrate of IRE1 kinase, SPL. Our data show that both intracellular S1P and mitochondrial S1P levels are reduced by IRE1 inhibition under stress conditions. Future studies could illuminate whether cytoplasmic or mitochondrial S1P or both is required for UPR[mt] induction in mammalian cells and how S1P coordinates the induction of the transcriptional and translational layers of UPR[mt]. The mice used in our study, Apoe^{-/-} mice, are known to have high level of lipids in the form of cholesterol and saturated fatty acids in their blood samples, especially after being fed with hyperlipidemic diet (58). Moreover, bioactive S1P is found to be higher in the plasma of Apoe^{-/-} mice in comparison to their WT counterparts (59). It is plausible that both the higher lipids and the higher S1P in the blood of Apoe^{-/-} mice could contribute to UPR[mt] activation in their livers. Another intriguing possibility is that S1P, being a secreted lipid mediator that travels in plasma (bound to high-density lipoprotein), could potentially communicate ER stress to distant tissues, but this needs future experimental validation (60). Indeed, a previous study showed that extrinsic S1P treatment can induce ER stress, but the study did not simultaneously assess UPR[mt] activation (61).

Our data also showed that ER stress engages UPR[mt] through eif2α phosphorylation. Numerous studies in mammalian cells showed that eif2α phosphorylation is required for the induction of UPR[mt] (17, 62). Unexpectedly, our data further showed that inhibition of IRE1 expression or kinase activity leads to the inhibition of two upstream eif2α kinases, mainly through inhibition of cytoplasmic PKR and to a lesser degree of ER-anchored PERK. Phosphorylation of eif2α leads to global translational attenuation but a few, select mRNAs escape to be translated during stress (51). Our findings are not the only one connecting the dots between these two kinases and mitochondria. For example, mitochondrial RNAs can form intermolecular double-stranded RNAs that have been shown to interact and activate PKR in the cytoplasm. The same study showed that PKR can also localize to mitochondria and the nucleus (63). In addition, prior studies have shown that PERK is required for ER and mitochondria contact sites, promotes protective mitochondrial hyperfusion, and inhibits mitophagy during ER stress (28, 54, 64). Moreover, it has been shown that ER stress-induced eif2α phosphorylation leads to translational downregulation of mRNAs encoding mitochondrial ribosomal proteins without changing their transcript levels (65). However, it is not known how UPR[ER] and ISR responses coordinate with mitochondrial translation to avoid a misalignment of nuclear-encoded and mitochondria-encoded proteins that assemble into mitochondrial complexes. A discoordination between these stress responses could trigger a mitochondrial proteotoxicity or disrupt mitochondrial energetics, tying into the activation of UPR[mt].

It is unclear how increasing the levels of intracellular S1P engages UPR[mt]. One possibility is that the regulation of S1P levels by IRE1 through the modulation of SPL activity may change the mitochondrial energetics and lead to the activation of UPR[mt]. In addition to its effect on mitochondrial Ca^{2+} uptake, localization of IRE1 to MAMs has been shown to modulate mitochondrial bioenergetics in mammalian cells (53). More recently, SPL has been shown to locate outer membrane of mitochondria in *Trypanosoma brucei* (66). Interaction between IRE1 and SPL which are shown to be in the proximity of mitochondria may provide another layer of control for mitochondrial S1P levels. Reduction in SPL activity under ER stress conditions may increase local S1P levels in mitochondria. S1P-produced in mitochondria by SPHK2 has been shown to bind to mitochondrial protein, PHB2. Interaction between mitochondrial S1P and PHB2 is important for cytochrome-c oxidase assembly and mitochondrial respiration (42).

Our data provide strong support for the central role of ER stress-induced IRE1-S1P axis in robust induction of UPR[mt] in mammalian cells. However, there could be additional ER stress-induced mechanisms that affect mitochondrial proteostasis. One mechanism could involve the disruption of ER surface-mediated (ER-SURF) mitochondrial protein targeting. In ER-SURF, the newly synthesized mitochondrial proteins are initially bound and stored on the ER surface. With the help of specialized ER chaperones, these mitochondrial proteins are re-routed to the mitochondria (67). While ER-SURF has not been studied in mammalian cells, the conservation of a critical protein in this pathway (encoded by EMA19 in yeast) suggests a similar mechanism is in action in mammalian cells. Hypothetically, the disruption of the mammalian counterpart of the ER-SURF pathway could initiate UPR[mt] by preventing the translocation of functional mitochondrial proteins to the mitochondria. This exciting possibility can be addressed by future studies focusing on understanding whether ER stress can prevent proper mitochondrial localization of certain proteins in mammalian cells. As S1P is a lipid mediator that is secreted to the extracellular environment and travels in plasma (bound to high-density lipoprotein), it can communicate ER stress to distant tissues (68). Indeed, extrinsic S1P treatment can induce ER stress (61).

It has been shown that IRE1 controls intercellular communication in *C. elegans*, but whether this is

---

protease-1; IRE1, inositol-requiring enzyme-1; MEFs, mouse embryonic fibroblasts; MF, mitochondrial fraction; mtHSP70, mitochondrial heat shock protein 70; LONP1, Lon protease-1; SPL, sphingosine 1-phosphate lyase; mt, mitochondria; TG, thapsigargin; UPR, unfolded protein response.
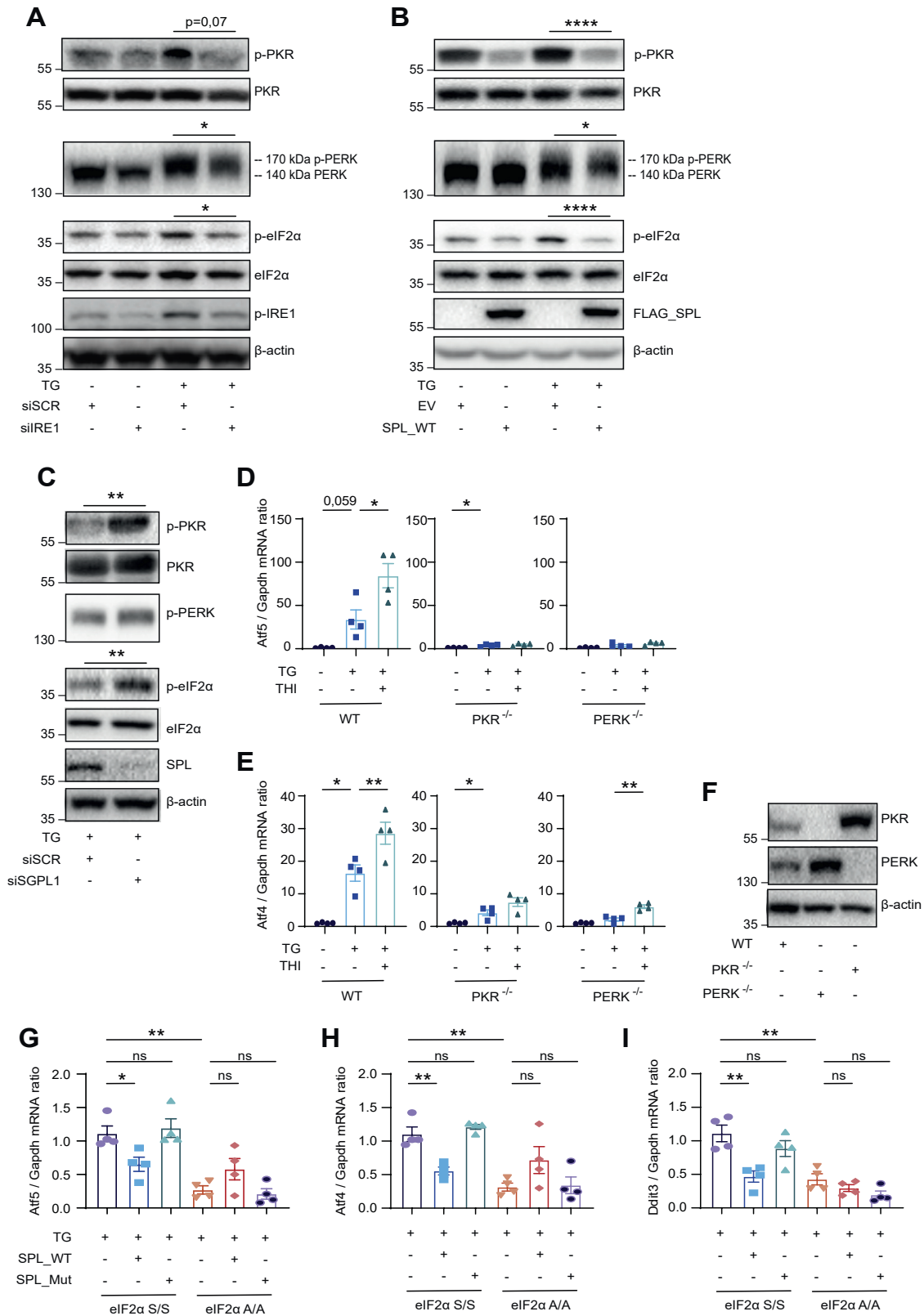
Fig. 7. Inhibition of IRE1-SPL axis prevents eif2α phosphorylation by suppressing PERK and PKR activation by ER stress. A: HEK293 cells were electroporated with either siSCR or siIRE1 (50 nM) for 48 h and then treated with TG (100 nM; 4 h). Protein lysates were analyzed by Western blotting using specific antibodies for PERK, p-PKR, PKR, p-eif2α, eif2α, pIRE1, and β-actin (n = 3 biological replicates). B: HEK293 cells were transfected by either empty vector or SPL_WT plasmids for 24 h and then treated with TG (100 nM; 8 h). Protein lysates were analyzed by Western blotting using specific antibodies for PERK, p-PKR, PKR, p-eif2α, eif2α, pIRE1, FLAG, and β-actin. (n = 3 biological replicates). C: HEK293 cells were electroporated with either siSCR or siIRE1 (50 nM) for 48 h and then treated with TG (100 nM; 4 h). Protein lysates were analyzed by Western blotting using specific antibodies for PERK,
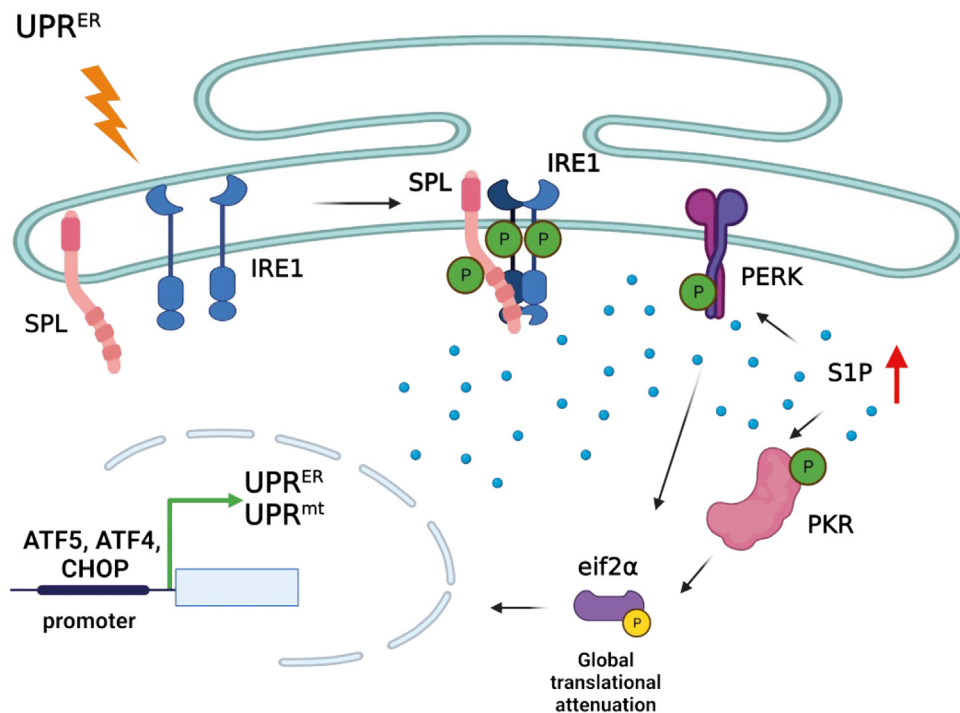
Fig. 8. IRE1-SPL axis impinges on eif2α phosphorylation through modulating PERK and PKR activities and establishes an additional layer of control over UPR^mt induction during ER stress in mammalian cells. Activated by ER stress, IRE1 phosphorylates SPL that is found on the ER membranes. IRE1-mediated phosphorylation leads to inactivation to SPL and increased S1P levels in cells. IRE1-SPL axis mainly regulates PKR activity and eif2α phosphorylation, a critical upstream event in the activation of mammalian UPR^mt signaling. ER, endoplasmic reticulum; IRE1, inositol-requiring enzyme-1; mt, mitochondria; PKR, double-stranded RNA-activated protein kinase; PERK, PKR–like ER kinase; SPL, sphingosine 1-phosphate lyase; UPR, unfolded protein response.

conserved in mammals and whether S1P plays a role in interorgan communication is not known (69). In *C. elegans,* neuronal IRE1 activation leads to the release of small vesicles carrying a secreted ER stress signal (SERSS) that is sensed by the intestinal cells and activates a cell nonautonomous signaling to enhance proteostasis and longevity (70, 71). Whether S1P is a SERSS in nematodes has not been investigated. Our findings suggest that S1P is poised to be an IRE1-regulated SERSS that could impact mitochondrial and ER proteostasis in distant body parts. It is known that circulating S1P promotes atherosclerosis. In plaques, ER and mitochondrial stress are known to play proinflammatory and proatherogenic roles (72–74). Of note, S1P is not the only circulating factor that is induced by UPR signaling in mammals. Other secreted factors include the fibroblast growth factor-21 that is induced by ATF4 and the growth/differentiation factor-15 that is induced by CHOP (75). In addition to revealing a new

layer in the complex regulation of mammalian proteostasis, our findings warrant future investigation into IRE1-mediated interorgan stress communication by secreted S1P.

Finally, while our study did not examine this thoroughly, data available in the literature support that hyperlipidemic conditions are accompanied with UPR^mt induction. For example, the expressions of UPR^mt-related transcription factors and chaperones/proteases were found to be significantly increased in fish livers under hyperlipidemic conditions in vivo (76). Furthermore, the hyperlipidemic induction of ATF4 and CHOP in mouse liver and adipose tissue has been extensively studied (77, 78). It has also been shown that ATF5 expression is induced by HFD in the subcutaneous adipose tissue of mice, and ATF5 expression correlated with increased adiposity in both mice and human (79). Additionally, lipid stress (induced by the addition of a saturated fatty acid, palmitate) effectively

induced the level of ATF4, ATF5, and CHOP in vivo ([28], [80]). Future studies will be needed to clarify whether UPR^{mt} is protective or damaging to the liver in hyperlipidemic conditions.

In summary, our results demonstrate a key role for mammalian IRE1 kinase in suppressing SPL activity to enhance intracellular S1P levels and augment UPR^{mt} signaling. These findings help define a new layer of control over UPR^{ER} and UPR^{mt} that is exerted by IRE1 kinase and which serves to orchestrate an integrated, robust response to ER stress.

Data Availability

All data are available in the main text or the supplementary materials. Research materials used in the article can be requested from authors. This study includes no data deposited in external repositories. ▯

Author ORCIDs

Asli D. Yildirim ⓘ https://orcid.org/0000-0002-5654-3093
Mevlut Citir ⓘ https://orcid.org/0000-0001-8715-9441
Asli E. Dogan ⓘ https://orcid.org/0000-0003-1546-7191
Zehra Yildirim ⓘ https://orcid.org/0000-0003-3132-8984
Ozlem Tufanli ⓘ https://orcid.org/0000-0003-4388-3571
Ebru Erbay ⓘ https://orcid.org/0000-0001-9584-1803

Conflict of Interest

The authors declare that they have no conflicts of interest with the contents of this article.

REFERENCES

1. Arrieta, A., Blackwood, E. A., Stauffer, W. T., and Glembotski, C. C. (2020) Integrating ER and mitochondrial proteostasis in the healthy and diseased heart. *Front. Cardiovasc. Med.* **6**, 193
2. Balch, W. E., Morimoto, R. I., Dillin, A., and Kelly, J. W. (2008) Adapting proteostasis for disease intervention. *Science.* **319**, 916
3. Wu, J., and Kaufman, R. J. (2006) From acute ER stress to physiological roles of the unfolded protein response. *Cell Death Differ.* **13**, 374–384
4. Walter, P., and Ron, D. (2011) The unfolded protein response: from stress pathway to homeostatic regulation. *Science.* **334**, 1081
5. Mori, K. (2009) Signalling pathways in the unfolded protein response: development from yeast to mammals. *J. Biochem.* **146**, 743–750
6. Bertolotti, A., Zhang, Y., Hendershot, L. M., Harding, H. P., and Ron, D. (2000) Dynamic interaction of BiP and ER stress transducers in the unfolded-protein response. *Nat. Cell Biol.* **2**, 326–332
7. Itzhak, D., Bright, M., McAndrew, P., Mirza, A., Newbatt, Y., Strover, J., *et al.* (2014) Multiple autophosphorylations significantly enhance the endoribonuclease activity of human inositol requiring enzyme 1α. *BMC Biochem.* **15**, 3
8. Shamu, C. E., and Walter, P. (1996) Oligomerization and phosphorylation of the Ire1p kinase during intracellular signaling from the endoplasmic reticulum to the nucleus. *EMBO J.* **15**, 3028–3039
9. Wu, R., Zhang, Q-H., Lu, Y-J., Ren, K., and Yi, G-H. (2015) Involvement of the IRE1α-XBP1 pathway and XBP1s-dependent transcriptional reprogramming in metabolic diseases. *DNA Cell Biol.* **34**, 6–18
10. Harding, H. P., Novoa, I., Zhang, Y., Zeng, H., Wek, R., Schapira, M., *et al.* (2000) Regulated translation initiation controls stress-induced gene expression in mammalian cells. *Mol. Cell.* **6**, 1099–1108
11. Ron, D., and Walter, P. (2007) Signal integration in the endoplasmic reticulum unfolded protein response. *Nat. Rev. Mol. Cell Biol.* **8**, 519–529
12. Barbosa, C., Peixeiro, I., and Romão, L. (2013) Gene expression regulation by upstream open reading frames and human disease. *PLoS Genet.* **9**, e1003529
13. Costa-Mattioli, M., and Walter, P. (2020) The integrated stress response: from mechanism to disease. *Science.* **368**, eaat5314
14. Webster, S. J., Ellis, L., O'Brien, L. M., Tyrrell, B., Fitzmaurice, T. J., Elder, M. J., *et al.* (2016) IRE1α mediates PKR activation in response to Chlamydia trachomatis infection. *Microbes Infect.* **18**, 472–483
15. Pickles, S., Vigié, P., and Youle, R. J. (2018) Mitophagy and quality control mechanisms in mitochondrial maintenance. *Curr. Biol.* **28**, R170–R185

ASBMB

16. Fischer, F., Hamann, A., and Osiewacz, H. D. (2012) Mitochondrial quality control: an integrated network of pathways. *Trends Biochem. Sci.* **37**, 284–292

17. Melber, A., and Haynes, C. M. (2018) UPRmt regulation and output: a stress response mediated by mitochondrial-nuclear communication. *Cell Res.* **28**, 281–295

18. Kang, P-J., Ostermann, J., Shilling, J., Neupert, W., Craig, E. A., and Pfanner, N. (1990) Requirement for hsp70 in the mitochondrial matrix for translocation and folding of precursor proteins. *Nature.* **348**, 137–143

19. Zhao, Q., Wang, J., Levichkin, I. V., Stasinopoulos, S., Ryan, M. T., and Hoogenraad, N. J. (2002) A mitochondrial specific stress response in mammalian cells. *EMBO J.* **21**, 4411–4419

20. Tatsuta, T., and Langer, T. (2009) AAA proteases in mitochondria: diverse functions of membrane-bound proteolytic machines. *Res. Microbiol.* **160**, 711–717

21. Aldridge, J. E., Horibe, T., and Hoogenraad, N. J. (2007) Discovery of genes activated by the mitochondrial unfolded protein response (mtUPR) and cognate promoter elements. *PLoS One.* **2**, e874

22. Fiorese, Christopher J., Schulz, Anna M., Lin, Y-F., Rosin, N., Pellegrino, Mark W., and Haynes, Cole M. (2016) The transcription factor ATF5 mediates a mammalian mitochondrial UPR. *Curr. Biol.* **26**, 2037–2043

23. Zhou, Donghui, Palam, L Reddy, Jiang, Li, Narasimhan, Jana, Staschke, Kirk A., and Wek, R. C. (2008) Phosphorylation of eIF2 directs ATF5 translational control in response to diverse stress conditions. *J. Biol. Chem.* **283**, 7064–7073

24. López-Crisosto, C., Bravo-Sagua, R., Rodriguez-Peña, M., Mera, C., Castro, P. F., Quest, A. F. G., *et al.* (2015) ER-to-mitochondria miscommunication and metabolic diseases. *Biochim. Biophys. Acta.* **1852**, 2096–2105

25. Moltedo, O., Remondelli, P., and Amodio, G. (2019) The mitochondria–endoplasmic reticulum contacts and their critical role in aging and age-associated diseases. *Front. Cell Dev. Biol.* **7**, 172

26. Hori, O., Ichinoda, F., Tamatani, T., Yamaguchi, A., Sato, N., Ozawa, K., *et al.* (2002) Transmission of cell stress from endoplasmic reticulum to mitochondria: enhanced expression of Lon protease. *J. Cell Biol.* **157**, 1151–1160

27. Han, J., Back, S. H., Hur, J., Lin, Y-H., Gildersleeve, R., Shan, J., *et al.* (2013) ER-stress-induced transcriptional regulation increases protein synthesis leading to cell death. *Nat. Cell Biol.* **15**, 481–490

28. Onat Umut, I., Yildirim Asli, D., Tufanli, Ö., Çimen, I., Kocatürk, B., Veli, Z., *et al.* (2019) Intercepting the lipid-induced integrated stress response reduces atherosclerosis. *J. Am. Coll. Cardiol.* **73**, 1149–1169

29. Yang, W., Tiffany-Castiglioni, E., Koh, H. C., and Son, I-H. (2009) Paraquat activates the IRE1/ASK1/JNK cascade associated with apoptosis in human neuroblastoma SH-SY5Y cells. *Toxicol. Lett.* **191**, 203–210

30. Acosta-Alvear, D., Karagöz, G. A-O., Fröhlich, F. A-O., Li, H. W., C, T., and Walter, P. A-O. X. (2018) The unfolded protein response and endoplasmic reticulum protein targeting machineries converge on the stress sensor IRE1. *Elife.* **7**, e43036

31. Serra, M., and Saba, J. D. (2010) Sphingosine 1-phosphate lyase, a key regulator of sphingosine 1-phosphate signaling and function. *Adv. Enzyme Regul.* **50**, 349–362

32. Kim, S., and Sieburth, D. (2018) Sphingosine kinase activates the mitochondrial unfolded protein response and is targeted to mitochondria by stress. *Cell Rep.* **24**, 2932–2945.e2934

33. Allen, J. J., Li, M., Brinkworth, C. S., Paulson, J. L., Wang, D., Hübner, A., *et al.* (2007) A semisynthetic epitope for kinase substrates. *Nat. Met.* **4**, 511–516

34. Bedia, C., Fau - Casas, J. Camacho L., Casas J Fau - Abad, J. L., Abad Jl Fau - Delgado, A., Delgado A Fau - Van Veldhoven, P. P., Van Veldhoven Pp Fau - Fabriàs, G., *et al.* (2009) Synthesis of a fluorogenic analogue of sphingosine-1-phosphate and its use to determine sphingosine-1-phosphate lyase activity. *Chembiochem.* **10**, 820–822

35. Zhang, D., and J. S. Armstrong. Bax and the mitochondrial permeability transition cooperate in the release of cytochrome c during endoplasmic reticulum-stress-induced apoptosis.

36. Polo, M., Alegre, F., Moragrega, A. B., Gibellini, L., Marti-Rodrigo, A., Blas-Garcia, A., *et al.* (2017) Lon protease: a novel mitochondrial matrix protein in the interconnection between drug-induced mitochondrial dysfunction and endoplasmic reticulum stress. *Br. J. Pharmacol.* **174**, 4409–4429

37. Ghosh, R., Wang, L., Wang, Eric S., Perera, B. Gayani K., Igbaria, A., Morita, S., *et al.* (2014) Allosteric inhibition of the IRE1α RNase preserves cell viability and function during endoplasmic reticulum stress. *Cell.* **158**, 534–548

38. Harnoss, J. M., Le Thomas, A., Shemorry, A., Marsters, S. A., Lawrence, D. A., Lu, M., *et al.* (2019) Disruption of IRE1α through its kinase domain attenuates multiple myeloma. *Proc. Natl. Acad. Sci. U. S. A.* **116**, 16420

39. Harrington, P. E., Biswas, K., Malwitz, D., Tasker, A. S., Mohr, C., Andrews, K. L., *et al.* (2015) Unfolded protein response in cancer: IRE1α inhibition by selective kinase ligands does not impair tumor cell viability. *A. C. S. Med. Chem. Lett.* **6**, 68–72

40. Tufanli, O., Telkoparan Akillilar, P., Acosta-Alvear, D., Kocaturk, B., Onat, U. I., Hamid, S. M., *et al.* (2017) Targeting IRE1 with small molecules counteracts progression of atherosclerosis. *Proc. Natl. Acad. Sci. U. S. A.* **114**, E1395

41. Urra, H., Pihan, P., and Hetz, C. (2020) The UPRosome - decoding novel biological outputs of IRE1alpha function. *J. Cell Sci.* **133**, jcs218107

42. Strub, G. M., Paillard, M., Liang, J., Gomez, L., Allegood, J. C., Hait, N. C., *et al.* (2011) Sphingosine-1-phosphate produced by sphingosine kinase 2 in mitochondria interacts with prohibitin 2 to regulate complex IV assembly and respiration. *FASEB J.* **25**, 600–612

43. Maharaj, A., Williams, J., Bradshaw, T., Güran, T., Braslavsky, D., Casas, J., *et al.* (2020) Sphingosine-1-phosphate lyase (SGPL1) deficiency is associated with mitochondrial dysfunction. *J. Steroid Biochem. Mol. Biol.* **202**, 105730

44. Hollien, J., Lin, J. H., Han, Li, Stevens, N., Walter, P., and Weissman, J. S. (2009) Regulated Ire1-dependent decay of messenger RNAs in mammalian cells. *J. Cell Biol.* **186**, 323–331

45. Papa, F. R., Zhang, K., Fau - Shokat, C., Shokat, P., Fau - Walter, K., and Walter, P. (2003) Bypassing a kinase activity with an ATP-competitive drug. *Science.* **302**, 1533–1537

46. Park, K., Ikushiro, H., Seo, H. S., Shin, K-O., Kim, Y.i., Kim, J. Y., *et al.* (2016) ER stress stimulates production of the key antimicrobial peptide, cathelicidin, by forming a previously unidentified intracellular S1P signaling complex. *Proc. Natl. Acad. Sci. U. S. A.* **113**, E1334

47. Bektas, M., Allende, M. L., Lee, B. G., Chen, W., Amar, M. J., Remaley, A. T., *et al.* (2010) Sphingosine 1-phosphate lyase deficiency disrupts lipid homeostasis in liver. *J. Biol. Chem.* **285**, 10880–10889

48. Di Pardo, A., Amico, E., Basit, A., Armirotti, A., Joshi, P., Neely, M. D., *et al.* (2017) Defective Sphingosine-1-phosphate metabolism is a druggable target in Huntington's disease. *Sci. Rep.* **7**, 5280

49. Lee, E-S., Yoon, C-H., Kim, Y-S., and Bae, Y-S. (2007) The double-strand RNA-dependent protein kinase PKR plays a significant role in a sustained ER stress-induced apoptosis. *FEBS Lett.* **581**, 4325–4332

50. McEwen, E., Kedersha, N., Song, B., Scheuner, D., Gilks, N., Han, A., *et al.* (2005) Heme-regulated inhibitor kinase-mediated phosphorylation of eukaryotic translation initiation factor 2 inhibits translation, induces stress granule formation, and mediates survival upon arsenite exposure. *J. Biol. Chem.* **280**, 16925–16933

51. Pakos-Zebrucka, K., Koryga, I., Mnich, K., Ljujic, M., Samali, A., and Gorman, A. M. (2016) The integrated stress response. *EMBO Rep.* **17**, 1374–1395

52. Zhang, P., McGrath Barbara, C., Reinert, J., Olsen DeAnne, S., Lei, L., Gill, S., *et al.* (2002) The GCN2 eIF2α kinase is required for adaptation to amino acid deprivation in mice. *Mol. Cell Biol.* **22**, 6681–6688

53. Carreras-Sureda, A., Jaña, F., Urra, H., Durand, S., Mortenson, D. E., Sagredo, A., *et al.* (2019) Non-canonical function of IRE1α determines mitochondria-associated endoplasmic reticulum composition to control calcium transfer and bioenergetics. *Nat. Cell Biol.* **21**, 755–767

54. Verfaillie, T., Rubio, N., Garg, A. D., Bultynck, G., Rizzuto, R., Decuypere, J. P., *et al.* (2012) PERK is required at the ER-mitochondrial contact sites to convey apoptosis after ROS-based ER stress. *Cell Death Differ.* **19**, 1880–1891

55. Hom, J. R., Gewandter, J. S., Michael, L., Sheu, S-S., and Yoon, Y. (2007) Thapsigargin induces biphasic fragmentation of

mitochondria through calcium-mediated mitochondrial fission and apoptosis. *J. Cell Physiol.* **212**, 498–508

56. Bronner, D. N., Abuaita, B. H., Chen, X., Fitzgerald, K. A., Nuñez, G., He, Y., *et al.* (2015) Endoplasmic reticulum stress activates the inflammasome via NLRP3- and Caspase-2-driven mitochondrial damage. *Immunity.* **43**, 451–462

57. Matsumoto, T., Uchiumi, T., Monji, K., Yagi, M., Setoyama, D., Amamoto, R., *et al.* (2017) Doxycycline induces apoptosis via ER stress selectively to cells with a cancer stem cell-like properties: importance of stem cell plasticity. *Oncogenesis.* **6**, 397

58. Rinne, P., Kadiri, J. J., Velasco-Delgado, M., Nuutinen, S., Viitala, M., Hollmén, M., *et al.* (2018) Melanocortin 1 receptor deficiency promotes atherosclerosis in Apolipoprotein E−/− Mice. *Arterioscler. Thromb. Vasc. Biol.* **38**, 313–323

59. Kurano, M., Tsukamoto, K., Hara, M., Ohkawa, R., Ikeda, H., and Yatomi, Y. (2015) LDL receptor and ApoE are involved in the clearance of ApoM-associated sphingosine 1-phosphate. *J. Biol. Chem.* **290**, 2477–2488

60. Cartier, A., and Hla, T. (2019) Sphingosine 1-phosphate: lipid signaling in pathology and therapy. *Science.* **366**, eaar5551

61. Huang, Y. L., Chang, C. L., Tang, C. H., Lin, Y. C., Ju, T. K., Huang, W. P., *et al.* (2014) Extrinsic sphingosine 1-phosphate activates S1P5 and induces autophagy through generating endoplasmic reticulum stress in human prostate cancer PC-3 cells. *Cell Signal.* **26**, 611–618

62. Haynes, C. M., and Ron, D. (2010) The mitochondrial UPR – protecting organelle protein homeostasis. *J. Cell Sci.* **123**, 3849–3855

63. Kim, Y., Park, J., Kim, S., Kim, M., Kang, M. G., Kwak, C., *et al.* (2018) PKR senses nuclear and mitochondrial signals by interacting with endogenous double-stranded RNAs. *Mol. Cell.* **71**, 1051–1063.e6

64. Lebeau, J., Saunders, J. M., Moraes, V. W. R., Madhavan, A., Madrazo, N., Anthony, M. C., *et al.* (2018) The PERK arm of the unfolded protein response regulates mitochondrial morphology during acute endoplasmic reticulum stress. *Cell Rep.* **22**, 2827–2836

65. Schneider, K., Nelson, G. M., Watson, J. L., Morf, J., Dalglish, M., Luh, L. M., *et al.* (2020) Protein stability buffers the cost of translation attenuation following eIF2α phosphorylation. *Cell Rep.* **32**, 108154

66. Dawoody Nejad, L., Stumpe, M., Rauch, M., Hemphill, A., Schneiter, R., Bütikofer, P., *et al.* (2020) Mitochondrial sphingosine-1-phosphate lyase is essential for phosphatidylethanol-amine synthesis and survival of Trypanosoma brucei. *Sci. Rep.* **10**, 8268

67. Hansen, K. G., Aviram, N., Laborenz, J., Bibi, C., Meyer, M., Spang, A., *et al.* (2018) An ER surface retrieval pathway safeguards the import of mitochondrial membrane proteins in yeast. *Science.* **361**, 1118

68. Cartier, A., and Hla, T. (2019) Sphingosine 1-phosphate: lipid signaling in pathology and therapy. *Science.* **366**

69. Imanikia, S., Sheng, M., and Taylor, R. C. (2018) Cell Non-autonomous UPR(ER) Signaling. *Curr. Top Microbiol. Immunol.* **414**, 27–43

70. Taylor, Rebecca C., and Dillin, A. (2013) XBP-1 is a cell-nonautonomous regulator of stress resistance and longevity. *Cell.* **153**, 1435–1447

71. Özbey, N. P., Imanikia, S., Krueger, C., Hardege, I., Morud, J., Sheng, M., *et al.* (2020) Tyramine acts downstream of neuronal XBP-1s to coordinate inter-tissue UPRER activation and behavior in C. elegans. *Dev. Cell.* **55**, 754–770.e756

72. Daum, G., Grabski, A., and MA, R. (2009) Sphingosine 1-phosphate: a regulator of arterial lesions. *Arterioscler. Thromb. Vasc. Biol.* **29**, 1439–1443

73. Erbay, E., Babaev, V. R., Mayers, J. R., Makowski, L., Charles, K. N., Snitow, M. E., *et al.* (2009) Reducing endoplasmic reticulum stress through a macrophage lipid chaperone alleviates atherosclerosis. *Nat. Med.* **15**, 1383–1391

74. Wang, Y., and I, T. (2014) Emerging roles of mitochondria ROS in atherosclerotic lesions: causation or association? *J. Atheroscler. Thromb.* **21**, 381–390

75. Bar-Ziv, R., Bolas, T., and Dillin, A. (2020) Systemic effects of mitochondrial stress. *EMBO Rep.* **21**, e50094

76. Song, Y-F., Zheng, H., Luo, Z., Hogstrand, C., Bai, Z-Y., and Wei, X-L. (2022) Dietary choline alleviates high-fat diet-induced hepatic lipid dysregulation via UPRmt modulated by SIRT3-mediated mtHSP70 deacetylation. *Int. J. Mol. Sci.* **23**, 4204

77. Wang, C., H, L., Meng Q, D. Y., Xiao, F., Zhang, Q., Yu J, L. K., *et al.* (2014) ATF4 deficiency protects hepatocytes from oxidative stress via inhibiting CYP2E1 expression. *J. Cell Mol. Med.* **8**, 80–90

78. Shin, J., He, M., Liu, Y., Paredes, S., Villanova, L., Brown, K., *et al.* (2013) SIRT7 represses Myc activity to suppress ER stress and prevent fatty liver disease. *Cell Rep.* **5**, 654–665

79. Zhao, Y., Zhang, Y-D., Zhang, Y-Y., Qian, S-W., Zhang, Z-C., Li, S-F., *et al.* (2014) p300-dependent acetylation of activating transcription factor 5 enhances C/EBPβ transactivation of C/EBPα during 3T3-L1 differentiation. *Mol. Cell Biol.* **34**, 315–324

80. Juliana, C. A., Yang, J., Rozo, A. V., Good, A., Groff, D. N., Wang, S-Z., *et al.* (2017) ATF5 regulates β-cell survival during stress. *Proc. Natl. Acad. Sci. U. S. A.* **114**, 1341–1346